Reduced-Order Modeling:
New Approaches for Computational Physics

Philip S. Beran [*]
Air Force Research Laboratory
Wright-Patterson Air Force Base, Ohio 45433-7531

Walter A. Silva [†]
NASA Langley Research Center
Hampton, Virginia 23681-0001

Abstract

In this paper, we review the development of new reduced-order modeling techniques and discuss their applicability to various problems in computational physics. Emphasis is given to methods based on Volterra series representations and the proper orthogonal decomposition. Results are reported for different nonlinear systems to provide clear examples of the construction and use of reduced-order models, particularly in the multi-disciplinary field of computational aeroelasticity. Unsteady aerodynamic and aeroelastic behaviors of two-dimensional and three-dimensional geometries are described. Large increases in computational efficiency are obtained through the use of reduced-order models, thereby justifying the initial computational expense of constructing these models and motivating their use for multi-disciplinary design analysis.

Introduction

Prior to the recent appearance of powerful digital computers, it was necessary to construct models of physical behaviors that took advantage of existing analytical techniques or which involved numerical calculations with small numbers of degrees of freedom (DOFs). Now, partial differential equations, representative of complex physics that were previously unobtainable, can be discretized and integrated with numerical algorithms implemented on massive parallel supercomputers. Indeed, the simulation of nonlinear physical behaviors in even three space dimensions has become relatively commonplace; problems with millions of DOFs can be routinely simulated, thereby allowing investigators to capture precisely important

phenomena. For example, as part of the Department of Energy's Accelerated Strategic Computing Initiative (ASCI), the world's fastest supercomputer (ASCI White - 12 trillion calculation per second) is being used in a shift from nuclear test-based methods to computation-based methods.

In the absence of other tools and analysis, numerical simulation is often insufficient in the knowing representation of complex physics. We see two main limitations of numerical simulation. First, while simulation can provide detailed time histories of discretized field variables, such data may not readily imbue the investigator with an increased level of understanding concerning the physics essential to a given phenomenon. As is true of physical experiment, careful analysis of the data is required to develop simpler models that can be used to predict important characteristics of system behavior. This process can be impeded by the enormous size of computed datasets. Second, without the dedication of massive resources, numerical simulation of large systems remains far too computationally expensive to be used in various multi-disciplinary settings, including control model synthesis, multi-variable optimization, and stability prediction. For example, in the field of computational fluid dynamics (CFD), codes for the simulation of turbulent, viscous flows in three space dimensions are often used to obtain point solutions, but less frequently used in related disciplines, such as aeroelasticity and shape optimization. Thus, there is a fundamental gap between the analysis fidelity available to simulate an individual case and that practical for multi-disciplinary analysis.

Both limitations of numerical simulation suggest that computed data need to be distilled into lower order models that can serve as the basis for additional analysis. The intent in constructing such reduced-order models (ROMs) is twofold: to provide quantitatively accurate descriptions of the dynamics of systems at a computational cost much lower than the original numerical model, and to provide a means by which system dynamics can be readily interpreted. We think

[*] Senior Research Aerospace Engineer, Structural Design and Development Branch, AFRL/VASD, Bldg. 146, 2210 Eighth Street, Wright-Patterson AFB OH 45433-7531; Associate Fellow of AIAA

[†] Senior Research Scientist, Aeroelasticity Branch, Mail Stop 340, NASA Langley Research Center, Hampton, VA 23681-0001; Senior Member of AIAA

of a low-order model as a characterization of a physical process, such that the essential behaviors of the process are captured with a relatively small number of DOFs. The use of point vortices to simulate the nonlinear dynamics of vorticity generating systems is a simple example of low-order modeling. ROMs are low-order models derived from some appropriate projection of a full systems DOFs to a much smaller set that encapsulates most, if not all, of the systems fundamental dynamics. Model accuracy typically depends on the number of retained DOFs and the convergence properties of the ROM. The reduction in computational cost needed to solve the ROM is offset by a potential loss of accuracy and model robustness.

The term "fidelity" is used to denote the degree to which a model captures the physics of a phenomenon of interest. Low fidelity implies that a computational model is missing key physical behaviors that render the model highly inaccurate in certain regimes, whereas high fidelity implies a broader range of model applicability. These terms alone are of ambiguous meaning, as they are dependent on the class of problems to which models are applied. For example, the linear potential equation can form a very accurate basis for computing loads in the subsonic regime, especially if corrected for viscous effects, but is a low-fidelity representation of flow behavior in the transonic regime, since leading-order (nonlinear) physical behavior is not properly modeled with this equation. Even in the subsonic regime, the linear potential equation may not be regarded to form the basis for a high-fidelity model if vehicles at large angles of attack are to be simulated. For a specified range of problem interest and physical behaviors, high-fidelity models capture the relevant physical behaviors using validated techniques to acceptable levels of accuracy. Thus, use of high-fidelity models usually leads to accurate solutions. However, application of a high-fidelity model is not sufficient for accuracy, owing to the need to execute properly the model on a computer (e.g., proper construction of a grid and selection of a time step).

One important trend driving the development of new ROM techniques is the increasing level of fidelity within multi-disciplinary analysis and design, which is a necessary consequence of the need for increased performance and reliability in many systems. The general purpose of reduced-order modeling is to lower the computational DOFs present in a numerical model while retaining the model's fidelity, i.e., the model's ability to capture physics of interest. Point simulations using high-fidelity equation sets (e.g., Navier-Stokes equations) typically cannot be obtained fast enough to permit design. This situation will improve, but at the same time, it is likely that models of even greater fidelity will be desired as more complex interaction physics are accounted for in simulation.

This paper reviews recent progress in the development of reduced-order modeling techniques and their application to multi-disciplinary problems, particularly in the area of computational aeroelasticity. The scope of the review is limited to the Volterra theory of nonlinear systems and the proper orthogonal decomposition (POD), which have been applied to the high-fidelity analysis of aeroelastic configurations in two and three space dimensions, and which show great potential for continued practical use. The remainder of this Introduction is devoted to an overview of these methods, while later in the paper, we describe applications of these methods beyond the field of aeroelasticity.

Volterra Theory of Nonlinear Systems

Over several decades of aerodynamics research, simple analytical models have given way to numerical descriptions of vehicle flight loads. This transition has been described by Silva,[1] which we summarize here. Early mathematical models of unsteady aerodynamic response capitalized on the efficiency and power of superposition of scaled and shifted fundamental responses, or convolution. Classical models of two-dimensional airfoils in incompressible flow[2] include Wagner's function (response to a unit step variation in angle of attack), Kussner's function (response to a sharp-edged gust in incompressible flow), Theodorsen's function (frequency response to sinusoidal motion), and Sear's function (frequency response to a sinusoidal gust). As geometric complexity increased, the analytical derivation of response functions was no longer practical and the numerical computation of linear unsteady aerodynamic responses in the frequency domain became the method of choice.[3] And, when geometry- and/or flow-induced nonlinearities became significant in the aerodynamic response of configurations of recent interest, the nonlinear equations were computed via time integration.

The trend towards time-domain numerical analysis of the aerodynamic equations has revealed the dynamics of numerous important and complex phenomena, but has not provided a framework for the analysis of complex configurations without severe computational costs. Aeroelastic analyses involving coupling of the nonlinear aerodynamic equations with the linear structural equations have been particularly costly to carry out. Post-processing of time transients at numerous flight conditions can be used to compute stability boundaries of the coupled system, but this approach has not been used extensively in industry due to the prohibitively high computational costs.

Attempts to address the problem of high computational cost include the development of transonic indicial responses.[4,5,6] Transonic indicial (step) responses are responses due to a step excitation of a particular input, such as angle of attack, about a transonic (or nonlinear) steady state condition. Neural net-

works have also been used to develop nonlinear models of unsteady aerodynamics[7] and nonlinear models of maneuvers (using an experimental database).[6] Neural networks and Volterra series have some similarities, since each involves the characterization of a system via an input-output mapping.[8,7] In particular, there is a direct relationship between the weights of a neural network and the kernels of a Volterra series representation for a particular system.[9]

A major difference between Volterra series and neural networks is in the training effort. Neural networks can require a substantial training effort[6] while Volterra series neither require a training period or curve fitting for model construction. Also, Volterra kernels provide a direct means for physical interpretation of a system's response characteristics in the time and frequency domains. However, potential disadvantages of the Volterra theory method include input amplitude limitations related to convergence issues and the need for higher order kernels.[1]

Another approach to reducing the computational cost of aerodynamic analysis with CFD is to restrict attention to linearized dynamics. The response of the linearized system about a nonlinear steady-state condition can be obtained with a linear state-space representation of the system at that condition. In this form, the order of the state-space model can be reduced using various techniques.[10,11] One method for building a linearized, low-order, frequency-domain model from CFD analysis is to apply the exponential (Gaussian) pulse input.[12] This method is used to excite the aeroelastic system, one mode at a time, using a broadband Gaussian pulse. The time-domain responses are transformed into the frequency domain to obtain a frequency-domain generalized aerodynamic force (GAF) influence coefficient matrix. These linearized GAFs can then be used in standard linear aeroelastic analyses.[13] Raveh, Levy and Karpel[14] apply this method while replacing the Gaussian pulse with step and impulse excitations. The responses to these alternate excitations can then be transformed into a state-space form for direct use in other disciplines such as controls or optimization.[15] We describe other frequency-domain representations in the context of the proper orthogonal decomposition.

However, in order to develop robust and efficient, nonlinear CFD-based ROMs that are mathematically correct, a rigorous method, well defined in the time and frequency domains for continuous- and discrete-time systems, is required. The Volterra theory of nonlinear systems fulfills these requirements. In particular, this theory has found wide application in the field of nonlinear discrete-time systems[16] and nonlinear digital filters for telecommunications and image processing.[17]

Application of nonlinear system theories, including the Volterra theory, to modeling nonlinear unsteady aerodynamic responses has not been extensive. One approach modeling unsteady transonic aerodynamic responses is Ueda and Dowell's[18] concept of describing functions, which is a harmonic balance technqiue involving one harmonic. Tobak and Pearson[19] apply the continuous-time Volterra concept of functionals to indicial (step) aerodynamic responses to compute nonlinear stability derivatives. Jenkins[20] also investigates the determination of nonlinear aerodynamic indicial responses and nonlinear stability derivatives using similar functional concepts. Stalford, Bauman, Garrett, and Herdman[21] develop Volterra models for simulating the behavior of a simplified nonlinear stall/post-stall aircraft model and the limit cycle oscillations of a simplified wing-rock model. In particular, they establish a straightforward analytical procedure for deriving the Volterra kernels from known nonlinear functions.

A particular response from a CFD code may provide information regarding the nonlinear aerodynamic behavior of a complex configuration due to a particular input at a particular flight condition. It does not, however, provide general information regarding the behavior of the configuration to a variation of the input, or the flight condition, or both. As a result, repeated use of the CFD code is necessary as input parameters and flight conditions are varied. A primary feature of the Volterra approach is the ability to characterize a linearized or nonlinear system using a small number of CFD-code analyses. Once characterized (via step or impulse responses of various orders), the functions can be implemented in a computationally efficient convolution scheme for prediction of responses to arbitrary inputs without the costly repeated use of the CFD code of interest. Characterization of the nonlinear response to an arbitrary input via the Volterra theory requires identification of the nonlinear Volterra kernels for a specified configuration and flight condition.

The problem of Volterra kernel identification is addressed by many investigators, including Rugh,[22] Clancy and Rugh,[23] Schetzen,[24] and more recently by Boyd, Tang, and Chua[25] and Reisenthel.[26] There are several ways of identifying Volterra kernels in the time and frequency domains that can be applied to continuous- or discrete-time systems. Tromp and Jenkins[27] use indicial (step) responses from a Navier-Stokes CFD code and a Laplace domain scheme to identify the first-order kernel of a pitch-oscillating airfoil. Rodriguez[28] generates realizations of state-affine systems, which are related to discrete-time Volterra kernels, for aeroelastic analyses. Assuming high-frequency response, Silva[29] introduces the concept of discrete-time, aerodynamic impulse responses, or kernels, for a rectangular wing under linear (subsonic) and nonlinear (transonic) conditions. Silva[30] improves upon these results by extending the methodology to arbitrary input frequencies, resulting in the first identification of discrete-time impulse responses of an aero-

dynamic system. It should be noted that owing to separation of the input terms, Silva's first approach had limited applicability for the identification of nonlinear Volterra kernels,[30] a situation which has been resolved more recently.[1]

In his dissertation, Silva[1] discusses the then prevailing misconceptions concerning aerodynamic impulse responses, including the purported difficulty in computing such responses. These misconceptions primarily arise from fundamental differences between traditional, continuous-time theories and modern discrete-time formulations. The appearance of discrete-time methods has great implications for aeroelasticity and aeroservoelasticity by providing a means for efficiently modeling nonlinear aerodynamics. In a similar fashion, other fields are likely to benefit from the coupling of large simulation codes and discrete-time response methods.

The Proper Orthogonal Decomposition

Before discussing the background of the proper orthogonal decomposition, as applied to large, discrete systems, we will first summarize the role POD often plays in computational physics. Reduced-order modeling with POD is essentially analysis by an empirical spectral method. With spectral methods, field variables are approximated using expansions involving chosen sets of basis functions. The governing equations are manipulated to obtain sets of equations for the coefficients of the expansions that can be solved to predict the behavior of field variables in space and time. The POD is an alternative basis that is derived from a set of system observations. In short, samples, or snapshots, of system behavior are used in a computation of appropriate sets of basis functions to represent system variables. The POD is remarkable in that the selection of basis functions is not just appropriate, but optimal, in a sense to be described further in the Analysis section.

The need to obtain samples of system behavior to construct the POD-based ROM is both a strength and a weakness of the method. One strength is that models can be efficiently tuned to capture physics in a high-fidelity manner. Two noteworthy weaknesses are the need to compute samples with a high-order, high-fidelity method, and the possible lack of model robustness to changes in parameters that govern system behavior. Generally, the payoff in applying POD is quite high when, following an initial investment of computation, a compact ROM can be constructed that can be used many times in, say, a multidisciplinary environment and which is valid over a useful range of system states.

The POD basis, otherwise known as the Karhunen-Loève basis,[31,32] is not new, but dates to the 1940s for continuous systems. Use of the POD is also known as principal-component analysis in the statistical litera-

ture.[33] In fluid mechanics, the POD was first applied to the study of turbulence and the analysis of turbulent flow data.[34,35] Numerous studies since then have employed POD to characterize the turbulent properties and dominant, or coherent, structures of wall-bounded flows and free shear layers using experimental data. This work, and much other activity related to the POD is thoroughly reviewed by Berkooz, Holmes and Lumley,[36] where references are given for early applications of POD in the fields of image processing, signal analysis, data compression, chemical engineering, and oceanography. Other references can be found in the fields of civil engineering[37,38] and structural dynamics.[39,40]

More recently, computational data has been used in the construction of POD bases. For example, Moin and Moser[41] used data from a numerically simulated channel flow to compute characteristic structures within the channel flowfield. Sirovich also put forth the method of snapshots (or strobes)[42] to ease the computational burden of obtaining the K-L basis for a discrete system. With the method of snapshots, eigenanalysis of an $M \times M$ matrix is carried out, where M is the number of snapshots, instead of an $N \times N$ matrix, where $N >> M$ is the number of data points in a snapshot. This process will be described in the Analysis section.

With the successful interpretation of large computational data sets using POD, the technique was extended to the dynamical modeling of various systems, including fluid-dynamical systems. Through this approach, for example, fluid-dynamical systems are first simulated with CFD techniques, samples are taken, a POD is constructed, and then a set of low-order equations is formulated in the POD basis, typically with a Galerkin projection, to study the dynamics of the system. Deane, Kevrekidis, Karniadakis and Orszag give an early example of this process as applied to flows through grooved channels and about circular cylinders.[43] In their noteworthy work, they successfully apply POD-based ROMs to the prediction of limit-cycle behavior in these systems. Other applications of POD to the dynamic modeling of nonlinear heat transfer and fluid dynamic problems can be found elsewhere.[44,45,46,47]

POD-based ROMs are now being developed for the analysis of aeroelastic systems. Romanowski authored the first paper, which appeared quite recently, documenting reduction of the aeroelastic equations using a K-L basis.[48] His time-domain procedure involved the construction of a low-order model for the linearized dynamics of an airfoil with structural coupling about nonlinear static states computed with the Euler equations. Subsequent to this work, frequency-domain procedures have appeared that more efficiently compute POD basis functions for linearized aeroelastic systems.[49,50] Work is also underway in the extension

of POD techniques to the analysis of problems in nonlinear aeroelasticity. Beran, Huttsell, Buxton, Noll and Osswald[51] proposed and tested a computational framework for computing static and dynamic behaviors of nonlinear systems with POD-based ROMs that Pettit and Beran[52,53] have extended to treat the discrete Euler equations. This work also forms the basis for an ongoing study of nonlinear panel response in the transonic regime.[54] Dowell, Thomas and Hall are also using POD techqniques to investigate the limit-cycle oscillation of an airfoil with a nonlinear structural coupling in the transonic regime.[55]

Analysis

In this section, we review important aspects of the analytical foundation of Volterra theory and the POD, as well as the application of reduced-order modeling techniques based on these methods to aerodynamic and aeroelastic systems. As described above, the POD is being applied in many different scientific and engineering disciplines, including aeroelasticity. While references are drawn from numerous sources, this review of POD analysis is not intended to be comprehensive, but is focused on recent work with connectivity to Air Force research activities.

We will restrict our attention to solution vectors in an N-dimensional, real, Euclidean space; these vectors will be written in boldface, along with the matrices used in vector equations. Time-dependent vectors of spatially discretized field variables, refered to as full-system vectors, are written as $\mathbf{w}(t)$, where t is time.

Volterra Theory

We begin by reviewing key features of the Volterra theory, as applied to time-invariant, nonlinear, continuous- and discrete-time systems. The literature on Volterra theory is rich, including several texts;[56,57,22,58] we follow the presentations of Silva[1,59] and Raveh, Levy and Karpel[14] to capture issues related to aeroelastic analysis. Furthermore, this section will concentrate on time-domain Volterra formulations, consistent with the implied application to time-domain, computational aeroelasticity methods; the foundations and applications of frequency-domain Volterra theory can be found elsewhere.[57,22,58,25]

While one goal of this work is to document the applicability of Volterra to discrete-time systems (e.g., systems arising in CFD), we first consider time-invariant, nonlinear, continuous-time, systems. Of interest is the response of the system about an initial state $\mathbf{w}(0) = \mathbf{W}_0$ due to an arbitrary input $u(t)$ (we take u as a real, scalar input, such as pitch angle of an airfoil) for $t \geq 0$. As applied to these systems, Volterra theory yields the response

$$\mathbf{w}(t) = \mathbf{h}_0 + \int_0^t \mathbf{h}_1(t - \tau)u(\tau)d\tau$$

$$+ \int_0^t \int_0^t \mathbf{h}_2(t - \tau_1, t - \tau_2)u(\tau_1)u(\tau_2)d\tau_1 d\tau_2 +$$

$$\sum_{n=3}^N \int_0^t .. \int_0^t \mathbf{h}_n(t - \tau_1, .., t - \tau_n)u(\tau_1)..u(\tau_n)d\tau_1 ..d\tau_n.$$

(1)

The Volterra series in expression (1) contains three classes of terms. The first is the steady-state term satisfying the initial condition, $\mathbf{h}_0 = \mathbf{W}_0$. Next is the first response term, $\int_0^\infty \mathbf{h}_1(t - \tau)u(\tau)d\tau$, where $\mathbf{h}$ is known as the first-order kernel (or the linear unit impulse response). The identification of the kernel $\mathbf{h}(\tau_1)$ is based on measuring the response of the system to a unit impulse (Dirac delta function) at $\tau_1 = 0$. Equation (1) requires the system to be time invariant, so that the system responds in an identical manner (but translated in time) to an impulse at any $\tau_1 > 0$. The first response term represents the convolution of the first-order kernel with the system inputs for times between 0 and t, where by causality, inputs beyond time t are excluded. Lastly are the higher order terms involving the second-order kernel, $\mathbf{h}_2$, and the nth-order kernels, $\mathbf{h}_n$. These terms do not all vanish when the system is nonlinear.[59] For example, identification of the second-order kernel is based on measuring the two-dimensional response of the system following impulse inputs at two different times. More will be said about kernel identification shortly.

The convergence of the Volterra series is dependent on input magnitude and the degree of system nonlinearity. Boyd[60] shows that the convergence of the Volterra series cannot be guaranteed when the maximum value of the input exceeds a critical value, which is system dependent. Of course, the issue of convergence is important, since the Volterra series must be truncated for analysis of practical systems. Silva[1,59] and Raveh et al.[14] consider a weakly nonlinear formulation, where it is assumed that the Volterra series can be accurately truncated beyond the second-order term:

$$\mathbf{w}(t) = \mathbf{h}_0 + \int_0^t \mathbf{h}_1(t - \tau)u(\tau)d\tau$$

$$+ \int_0^t \int_0^t \mathbf{h}_2(t - \tau_1, t - \tau_2)u(\tau_1)u(\tau_2)d\tau_1 d\tau_2. \quad (2)$$

The assumption of a weakly nonlinear system is consistent with the emergence of limit-cycle oscillation of a 2-D aeroelastic system in transonic flow through a supercritical Hopf bifurcation.[51] For linear systems, only the first-order kernel is non-trivial, and there are no limitations on input amplitude.

Silva[1] derives the first- and second-order kernels, which are presented here in final form in terms of various response functions:

$$\mathbf{h}_1(\tau_1) = 2\mathbf{w}_0(\tau_1) - \frac{1}{2}\mathbf{w}_2(\tau_1), \quad (3)$$

$$\mathbf{h}_2(\tau_1, \tau_2) = \frac{1}{2}\left(\mathbf{w}_1(\tau_1, \tau_2) - \mathbf{w}_0(\tau_1) - \mathbf{w}_0(\tau_2)\right). \quad (4)$$

In (3), $\mathbf{w}_0(\tau_1)$ is the time response of the system to a unit impulse applied at time 0 and $\mathbf{w}_2(\tau_1)$ is the time response of the system to an impulse of twice unit magnitude at time 0. These response functions represent the memory of the system. If the system is linear, then $\mathbf{w}_2 = 2\mathbf{w}_0$ and $\mathbf{h}_1 = \mathbf{w}_0$, which is why the first-order kernel is refered to as the linear unit impulse response. The identification of the second-order kernel is more demanding, since it is dependent on two parameters. Assuming $\tau_2 > \tau_1$ in (4), $\mathbf{w}_0(\tau_2)$ is the response of the system to an impulse at time τ_2.

Time is discretized with a set of time steps of equivalent size. Time levels are indexed from 0 (time 0) to n (time t), and the evaluation of $\mathbf{w}$ at time level n is denoted by $\mathbf{w}[n]$. The convolution in discrete time is

$$\mathbf{w}[n] = \mathbf{h}_0 + \sum_{k=0}^{N} \mathbf{h}_1[n-k]u[k]$$
$$+ \sum_{k_1=0}^{N} \sum_{k_2=0}^{N} \mathbf{h}_2[n-k_1, n-k_2]u[k_1]u[k_2]. \quad (5)$$

It should be noted that an important conceptual breakthrough in the development and application of the discrete-time Volterra theory as a ROM technique is understanding the fundamental difference between a continuous-time unit impulse response and a discrete-time unit impulse response.[1,59] The continuous-time unit impulse response is a highly abstract function which suffers from a difficult, if not impossible, practical (i.e., numerical) application. The discrete-time unit impulse response (also known as a unit sample response), on the other hand, is specifically designed for discrete-time (i.e., numerical) applications. The proof of this and details regarding the very powerful unit sample response can be found in any modern text on digital signal processing.[61]

The identification of linearized and nonlinear Volterra kernels is an essential step in the development of ROMs based on Volterra theory, but it is not the final step. Ultimately, these functional kernels can be transformed into linearized and nonlinear (bilinear) state-space systems that can be easily implemented into other disciplines such as controls and optimization.[22,1] Currently, research is underway to develop these models, and results should be available soon.[15]

In addition, some very interesting and fundamental research in the area of frequency-domain Volterra theory[62] and experimental applications of Volterra methods as applied to nonlinear aeroelastic problems[63] continues.

Proper Orthogonal Decomposition (POD)

POD is a linear method for establishing an optimal basis, or modal decomposition, of an ensemble of continuous or discrete functions. Detailed derivations of the POD and its properties are available elsewhere[64,65] and not repeated herein. In our discussion of POD, M basis vectors are used to represent deviations of $\mathbf{w}(t)$ from a base solution, $\mathbf{W}_0$. These are written as $\{\mathbf{e}^1, \mathbf{e}^2, ..., \mathbf{e}^M\}$, and are referred to by many names, including POD vectors,[50] empirical eigenfunctions[64] or, simply, modes.[64,52] For the sake of brevity, we shall use the term "modes" to denote the POD basis vectors. The modes are orthonormal

$$\mathbf{e}^{iT}\mathbf{e}^j = \begin{cases} 1 \text{ if } i = j \\ 0 \text{ otherwise,} \end{cases} \quad (6)$$

and computed in a manner to be described shortly. The modal decomposition of $\mathbf{w}$ using M modes is given by

$$\mathbf{w} \approx \mathbf{W}_0 + \sum_{i=1}^{M} \hat{w}_i \mathbf{e}^i = \mathbf{W}_0 + \mathbf{\Phi}\hat{\mathbf{w}}, \quad (7)$$

where $\mathbf{\Phi}$ is an $N \times M$ matrix containing the ordered set of modes, $\mathbf{\Phi} = \left[\mathbf{e}^1, \mathbf{e}^2, ..., \mathbf{e}^M\right]$ and $\hat{\mathbf{w}}$ is an M-dimensional vector of modal amplitudes, $\hat{\mathbf{w}} = [\hat{w}_1, \hat{w}_2, ..., \hat{w}_M]$. As a time-varying function, $\mathbf{w}$ is approximated by $\mathbf{W}_0 + \mathbf{\Phi}\hat{\mathbf{w}}(t)$.

As stated by Holmes et al.,[64] "Linearity is the source of the [POD] method's strengths as well as its limitations ..." The method is linear owing to the independence of the modes from the modal amplitudes, thereby allowing for the straightforward construction of reduced-order equation sets from the full equation sets following mode computation.

The POD modes are constructed by first computing samples, or snapshots, of system behavior (solutions at different instants in time for dynamic problems, or equilibrium solutions at different parameter values for static problems) and storing these samples in a snapshot matrix, $\mathbf{S}$. For now, we assume that M snapshots are collected and column-wise collocated into the $N \times M$ snapshot matrix: $\mathbf{S} = \left[\mathbf{w}^1, \mathbf{w}^2, ..., \mathbf{w}^M\right]$. By assumption, the snapshot matrix represents a random vector class of signals associated with the system. The basis provided by the POD, known as the Karhunen-Loève[31,32] (or K-L) basis, minimizes the error in approximating a member of this class with fewer than M basis vectors. This property of optimal convergence associated with the K-L basis is established in many works.[64,65,66,67,50] The K-L basis can be readily computed by relating the mode matrix to the snapshot matrix through a transformation matrix V, $\mathbf{\Phi} = \mathbf{S}\mathbf{V}$, maximizing the projection of the snapshot matrix onto the POD basis. This leads to the eigenproblem

$$\mathbf{S}^T\mathbf{S}\mathbf{V} = \mathbf{V}\mathbf{\Lambda} \quad (8)$$

for eigenvectors $\mathbf{V}$ and eigenvalues $\mathbf{\Lambda} = diag(\lambda_i)$. The eigenvalues are non-negative, since $\mathbf{S}^T\mathbf{S}$ is symmetric and positive semi-definite. Provided that the eigenvectors $\mathbf{V}$ are scaled to be orthonormal, $\mathbf{V}^T\mathbf{V} = \mathbf{I}$ ($\mathbf{I}$ is the

identity matrix), the transformation formula $\Phi = SV$ yields $\Phi^T\Phi = \Lambda$. Multiplying each e^i by $\sqrt{\lambda_i}$ yields an orthonormal set of modes, $\Phi^T\Phi = I$, as originally specified. It should be noted that for their frequency domain analysis, Hall et al. construct complex modes from $S^H SV = V\Lambda$, where S^H is the complex conjugate of the transpose of S.

In practice, fewer than M modes are retained to simulate system behavior. These are selected based on the size of the modal eigenvectors. Simply put, the K-L basis for a subspace of dimension $M_r < M$ is obtained by retaining the modes associated with the M_r largest eigenvalues computed in (8). It should also be noted that K-L theory establishes the K-L basis to be the eigenvectors of SS^T/M, where SS^T is the snapshot covariance matrix. Manipulation of (8) yields $SS^T\Phi = \Phi\Lambda$, and from the singular value decomposition of S, M eigenvalues are equivalent to those in Λ, while the other $N - M$ eigenvalues vanish (for finite-dimensional problems of dimension N).[68] Computation of V followed by evaluation of $\Phi = SV$ much more efficiently yields the POD modes than explicit analysis of the covariance matrix. In the following, we will consider the number of modes retained to be a variable denoted by M that is less than equal to the number of snapshots in S.

The techniques described below provide different means for obtaining reduced-order equations sets governing $w(t)$ in the POD subspace. There are several methods for accomplishing the projection, including the Galerkin projection, "subspace" projection (for linear and nonlinear systems), and collocation. We will explore the former two approaches herein.

Governing Equations

We place the nonlinear and spatially discretized, full-system equations in first-order form:

$$\frac{d\mathbf{w}}{dt} = \mathbf{R}(\mathbf{w}; \lambda), \tag{9}$$

where $\mathbf{w}$ is an array of variables associated with interior evaluation points (e.g., cell centers) throughout a computational domain, λ is a free parameter (or set of parameters), $\mathbf{R}$ is an array of nonlinear functions of the discrete variables, and t is time. For the discrete Euler equations in two space dimensions and conservative form, $\mathbf{w}$ is a collocation of density, two components of momentum, and total energy, involving $N = 4N_p$ variables, where N_p is the number of interior evaluation points. We also define an array of variables associated with boundary grid points (so-called ghost points), $\mathbf{w}_b$, that are referenced in the evaluation of $\mathbf{R}$ but not explicitly carried as variables. The $4N_b$ boundary conditions are specified in general form as

$$\mathbf{B}(\mathbf{w}, \mathbf{w}_b) = \mathbf{f}(t), \tag{10}$$

where $\mathbf{B}$ can be nonlinear in $\mathbf{w}$ and $\mathbf{w}_b$, and $\mathbf{f}$ is a time-dependent array representative of an evolving bound-

ary state. When $\mathbf{f}$ vanishes, equilibrium states, $\mathbf{W}$, of (9) exist and satisfy $\mathbf{R}(\mathbf{W}; \lambda) = \mathbf{0}$ and $\mathbf{B}(\mathbf{W}, \mathbf{W}_b) = \mathbf{0}$.

Linear (Frequency Domain) POD Formulation

Rapid progress has been made in the application of POD to aerodynamic and aeroelastic equation sets using a linear POD formulation.[50] The basic approach is to develop POD-based ROMs for the linearized dynamics about equilibrium solutions of the fully nonlinear equations, (9). For a given value of λ (e.g., Mach number), the nonlinear base solution is computed with CFD methods accelerated for steady-state conditions. The governing equations are then linearized for periodic disturbances of small amplitude, placed in frequency-domain form, and solved using similarly accelerated CFD methods. Solutions of the linearized equations, gathered for a range of different frequencies, serve as snapshots in the construction of a POD-based, linear ROM. Furthermore, a linearized ROM representative of the aerodynamics, can be attached to a set of nonlinear structural dynamic equations to form a compact, nonlinear aeroelastic model.[69,50]

Following Hall et al.,[50] a small disturbance to the equilibrium state is introduced:

$$\mathbf{w}(t; \lambda) = \mathbf{W}(\lambda) + \mathbf{q}e^{j\omega t}, \tag{11}$$

where ω is the disturbance frequency, $\mathbf{q}$ is a disturbance of small amplitude, j is the imaginary number. The disturbance is a response to forced oscillation about the equilibrium state at the boundary (e.g., a response in fluid velocity to the time rate-of-change of angle-of-attack for a pitching airfoil):

$$\mathbf{B}(\mathbf{w}, \mathbf{w}_b) = \frac{d}{dt}\mathbf{b}e^{j\omega t} = j\omega\mathbf{b}e^{j\omega t}, \tag{12}$$

where $\mathbf{b}$ represents the type of forcing applied to the system. Introducing $\mathbf{w}_b = \mathbf{W}_b + \mathbf{q}_b e^{j\omega t}$ leads to a small-disturbance boundary equation (assuming the invertability of $\frac{\partial \mathbf{B}}{\partial \mathbf{w}_b}$):

$$\frac{\partial \mathbf{B}}{\partial \mathbf{w}_b}\mathbf{q}_b = j\omega\mathbf{b} - \frac{\partial \mathbf{B}}{\partial \mathbf{w}}\mathbf{q}. \tag{13}$$

This equation is coupled to the small-disturbance form of the governing equation,

$$\mathbf{J}\mathbf{q} + \frac{\partial \mathbf{R}}{\partial \mathbf{w}_b}\mathbf{q}_b = j\omega\mathbf{q} \tag{14}$$

where $\mathbf{J} \equiv \frac{\partial \mathbf{R}}{\partial \mathbf{w}}$ is the system Jacobian (an $N \times N$ real matrix). Combining both sets of equations yields

$$\mathbf{A}\mathbf{q} = j\omega\tilde{\mathbf{b}}, \tag{15}$$

$$\mathbf{A} \equiv \frac{\partial \mathbf{R}}{\partial \mathbf{w}_b}\frac{\partial \mathbf{B}}{\partial \mathbf{w}_b}^{-1}\frac{\partial \mathbf{B}}{\partial \mathbf{w}} + j\omega\mathbf{I}, \quad \tilde{\mathbf{b}} \equiv \frac{\partial \mathbf{R}}{\partial \mathbf{w}_b}\frac{\partial \mathbf{B}}{\partial \mathbf{w}_b}^{-1}\mathbf{b}.$$

The solution of (15), $\mathbf{q}$, is a function of the forcing frequency, ω, and the character and amplitude of the forcing as expressed through $\mathbf{b}$.

It should be noted that (15) is based solely on the spatial discretization leading to $\mathbf{R}$ and does not account for the iterative character of numerical schemes by which $\mathbf{q}$ is computed. For example, Hall et al. obtain an equation with structure equivalent to that of (15) using an explicit, cell-centered, finite-volume Godunov method, but derive an expression for a Lax-Wendroff scheme that contains additional terms which are second order in ω.[50]

The POD is constructed using M solutions $\mathbf{q}^i (i = 1, ..., M)$ of (15), for different frequencies and forcing conditions (e.g., airfoil pitch and airfoil plunge), as column entries in the complex snapshot matrix, $\mathbf{S}$.[50] As has been reported, accuracy can be retained while keeping M quite small; M is typically between 10 and 100. Approximately half of the solutions need not be computed from (15), since solutions $\mathbf{q}$ at negative frequencies are complex conjugates of those at positive frequencies. The complex mode matrix $\mathbf{\Phi}$ is computed by first solving the complex form of (8), and then forming the product $\mathbf{SV}$. To predict the time-dependent response about the equilibrium state, $\mathbf{q}$ is approximated by $\mathbf{\Phi}\hat{\mathbf{q}}$ ($\hat{\mathbf{q}}$ is the array of reduced-order variables) and substituted into the small-disturbance equation (15): $\mathbf{A\Phi}\hat{\mathbf{q}} = j\omega\tilde{\mathbf{b}}$. Hall et al.[50] project this equation onto the space spanned by $\mathbf{\Phi}$ to obtain a reduced-order set of equations:

$$\hat{\mathbf{A}}\hat{\mathbf{q}} = j\omega\hat{\mathbf{b}} \quad \left(\hat{\mathbf{A}} \equiv \mathbf{\Phi}^H \mathbf{A}\mathbf{\Phi}, \ \hat{\mathbf{b}} \equiv \mathbf{\Phi}^H \tilde{\mathbf{b}}\right). \quad (16)$$

Returning to the original system, (15), we see the advantage of the POD formulation. If several solutions of (15) are required for different forcing conditions, the matrix $\mathbf{A}$ may be $\mathcal{LU}$-decomposed or may be analyzed for eigenmodes that will dominate in the predicted response. Such "up-front" computations reduce the per unit computational cost of solutions beyond the first, but become impractical when N becomes sufficiently large, since the computational effort grows at a much faster rate than the number of equations. For example, on square computational domains, the decomposition of $\mathbf{A}$ grows as N^2.

With POD, the up-front cost is far less than that just described. The empirical eigenvectors are computed once in no more than $\mathcal{O}(NM^2)$ operations (the product $\mathbf{S}^H\mathbf{S}$). These eigenvectors are used in the construction of $\hat{\mathbf{A}}$, which also requires $\mathcal{O}(NM^2)$ operations (assuming $\mathbf{A}$ is not explicitly formed, but implied through the computation of $\mathbf{A\Phi}_i$ as suggested by Hall et al.[50]). In practice, M is sufficiently small that the work is dominated by computation of the snapshots, a process requiring $\mathcal{O}(NM)$ operations. Furthermore, for a specified level of accuracy, M does not typically grow with N; i.e., beyond a nominal threshold, grid refinement does not better capture low-frequency, high-energy structures. Once (16) is formed through a set of transformations involving the empirical eigenvectors, many different cases ($\mathcal{O}(N)$) can be examined

at a commensurate cost, owing to the smallness of $\hat{\mathbf{A}}$ (an $M \times M$ matrix). Accuracy of the approach is high, provided that a sufficient number of modes are retained, and provided that the forcing conditions are within the scope of the sampling process.

The POD approach is well-suited to multi-disciplinary analysis involving repeated interactions between equation sets. A POD-based ROM can be used to simplify a computationally demanding equation set so that it can be efficiently integrated with a simpler equation set. For example, Hall et al. apply their analysis to the study of an isolated airfoil in transonic flow with pitch (α) and plunge (h) structural coupling.[50] Their development is now summarized. Following collocation of the structural variables into the array $\mathbf{h} = (h, \alpha)^T$, the structural dynamic equations are expressed as

$$\begin{bmatrix} -\mathbf{I} & \mathbf{0} \\ \mathbf{0} & \mathbf{M} \end{bmatrix} \frac{d}{dt} \begin{bmatrix} \mathbf{h} \\ \dot{\mathbf{h}} \end{bmatrix} + \begin{bmatrix} \mathbf{0} & \mathbf{I} \\ \mathbf{K} & \mathbf{0} \end{bmatrix} \begin{bmatrix} \mathbf{h} \\ \dot{\mathbf{h}} \end{bmatrix} = \begin{bmatrix} \mathbf{0} \\ \mathbf{F(w)} \end{bmatrix}, \quad (17)$$

where $\mathbf{M}$ is a 2×2 matrix containing the airfoil mass, static imbalance and moment of inertia (about the elastic axis), $\mathbf{K}$ is the 2×2 stiffness matrix, $\mathbf{F}$ is an array representing the integration of the discrete flowfield into an applied force and moment, and $\dot{\mathbf{h}} = \frac{d\mathbf{h}}{dt}$).

Here, (17) is placed in small-disturbance form assuming that aeroelastic equilibrium is achieved when $\mathbf{h} = 0$, such that $\mathbf{h} = \mathbf{h}_0 e^{j\omega t}$ and $\dot{\mathbf{h}} = j\omega\mathbf{h}_0 e^{j\omega t}$. The force and moment function is written as $\mathbf{F} = \mathbf{Cq}e^{j\omega t}$, where $\mathbf{q}$ is the flowfield disturbance captured by the aerodynamic equations. $\mathbf{C}$ is a sparse $2 \times N$ matrix that represents the discrete force and moment integration; it is a function of the reduced velocity ($V = U_\infty/\omega_\alpha b\sqrt{\mu}$, where U_∞ is the freestream velocity, ω_α is the pitch natural frequency, b is the airfoil semi-span, and μ is the airfoil-fluid mass ratio). Using a POD-based ROM, suitably trained for pitch and plunge oscillations, the disturbance $\mathbf{q}$ is replaced by a set of reduced-order variables as shown above: $\mathbf{q} = \mathbf{\Phi}\hat{\mathbf{q}}$. In small-disturbance form, (17) becomes

$$\begin{bmatrix} \mathbf{0} & \mathbf{I} \\ \mathbf{K} & \mathbf{0} \end{bmatrix} \begin{bmatrix} \mathbf{h}_0 \\ \dot{\mathbf{h}}_0 \end{bmatrix} + j\omega \begin{bmatrix} -\mathbf{I} & \mathbf{0} \\ \mathbf{0} & \mathbf{M} \end{bmatrix} \begin{bmatrix} \mathbf{h}_0 \\ \dot{\mathbf{h}}_0 \end{bmatrix} = \begin{bmatrix} \mathbf{0} \\ \mathbf{C\Phi}\hat{\mathbf{q}} \end{bmatrix}. \quad (18)$$

Pitch and plunge variables are linked to the aerodynamic disturbance problem by defining a sparse $N \times 2$ transformation matrix $\tilde{\mathbf{B}}$ such that $\tilde{\mathbf{b}} \equiv \tilde{\mathbf{B}}\mathbf{h}$. Thus, (16) becomes $\hat{\mathbf{A}}\hat{\mathbf{q}} - j\omega\mathbf{\Phi}^H\tilde{\mathbf{B}}\mathbf{h} = 0$, leading to a coupled set of $M + 4$ equations:

$$\begin{bmatrix} \hat{\mathbf{A}} & \mathbf{0} & \mathbf{0} \\ \mathbf{0} & \mathbf{0} & \mathbf{I} \\ -\mathbf{C\Phi} & \mathbf{K} & \mathbf{0} \end{bmatrix} \begin{bmatrix} \hat{\mathbf{q}} \\ \mathbf{h}_0 \\ \dot{\mathbf{h}}_0 \end{bmatrix}$$
$$+ j\omega \begin{bmatrix} \mathbf{0} & -\mathbf{\Phi}^H\tilde{\mathbf{B}} & \mathbf{0} \\ \mathbf{0} & -\mathbf{I} & \mathbf{0} \\ \mathbf{0} & \mathbf{0} & \mathbf{M} \end{bmatrix} \begin{bmatrix} \hat{\mathbf{q}} \\ \mathbf{h}_0 \\ \dot{\mathbf{h}}_0 \end{bmatrix} = 0. \quad (19)$$

Equation (19) represents a complex, general eigenvalue problem (for $\beta = j\omega$) of small size that can be used to compute the stability properties of the aeroelastic system with great efficiency. For a given airfoil configuration, the flutter speed can be bracketed by systematically varying reduced velocity as a parameter until the eigenvalue with largest real part changes sign. This approach can be contrasted with the direct approach of Morton and Beran,[70,71,72] which has been successfully applied to the prediction of airfoil flutter speeds in the transonic regime. Their direct method does not reduce the number of degrees of freedom in the solution array, and amounts to an implicit analysis of the eigensystem $\beta \mathbf{q} = \mathbf{Jq}$, which is expanded to include the structural equations. However, the method does search for a single, conjugate pair of eigenvectors that becomes neutrally stable, and with this restriction, allows flutter speeds to be predicted at a computational rate comparable to that of solving the nonlinear equations for the static base solution. As will be further reported in the Results section, the POD-based approach extends nicely into three dimensions,[73] while much additional work in this direction is required for the direct approach.

Nonlinear POD Formulation - Subspace Projection

The linear POD formulation described above provides a practical means for assessing the linear stability and dynamics of complex, aeroelastic systems at a very small fraction of the computational cost of full-system analysis. Specific examples will be given in the Results Section. In cases where the dynamics are nonlinear, or in which a reduced-order model of the nonlinear, static behavior is desired, a different class of methods is required. Two methods are described for treating nonlinear systems with POD: a subspace projection technique[51,52] and the Galerkin projection technique. The former is described in this section, while the latter is treated in the following section. The following development assumes that computed fields are reasonably smooth; the issue of field discontinuities is partially addressed later.

Equation (9) is projected onto the subspace of reduced-order variables through a weighted-residual approach.[74] The dynamic residual, $\mathcal{R}$, is defined as

$$\mathcal{R} \equiv \frac{d\mathbf{w}}{dt} - \mathbf{R}(\mathbf{w}; \lambda),$$

which, when forced to vanish after weighting by each of the M modes, yields

$$\Phi^T \left(\frac{d\mathbf{w}}{dt} - \mathbf{R}(\mathbf{W}_0 + \Phi\hat{\mathbf{w}}; \lambda) \right) = 0. \qquad (20)$$

With $\Phi^T\Phi = \mathbf{I}$, (20) takes a form equivalent to that previously applied by Pettit and Beran:[52]

$$\frac{d\hat{\mathbf{w}}}{dt} = \Phi^T \mathbf{R}(\mathbf{W}_0 + \Phi\hat{\mathbf{w}}; \lambda). \qquad (21)$$

Equilibrium solutions of (21) satisfy the equation

$$\hat{\mathbf{R}} \equiv \Phi^T \mathbf{R}(\mathbf{W}_0 + \Phi\hat{\mathbf{w}}; \lambda) = 0. \qquad (22)$$

This system of M nonlinear equations can be efficiently solved with the chord method following computation of the Jacobian, $\hat{\mathbf{J}} \equiv \frac{\partial \hat{\mathbf{R}}}{\partial \hat{\mathbf{w}}}$.[51] With this approach, the Jacobian is numerically computed about a specified state, $\mathbf{w}^0$, and then frozen in the iterative procedure $\hat{\mathbf{J}}(\mathbf{w}^0)\left(\hat{\mathbf{w}}^{\nu+1} - \hat{\mathbf{w}}^\nu\right) = -\hat{\mathbf{R}}$, where the superscript index denotes iteration. Only $\mathcal{O}(M)$ evaluations of $\mathbf{R}$ and $\Phi\hat{\mathbf{w}}$ are necessary to construct $\hat{\mathbf{J}}$. For the results presented below, chord iterates are continued until $\|\hat{\mathbf{R}}\| < 10^{-3}$ or a lack of convergence is demonstrated.

Unsteady solutions, $\hat{\mathbf{w}}(t)$, of (21) can be time integrated using either explicit or implicit techniques. As described further below, results have recently been presented[75] for integration with the second-order-accurate Crank-Nicolson scheme:[76]

$$\hat{\mathbf{F}}(\hat{\mathbf{w}}^{n+1}) \equiv \hat{\mathbf{w}}^{n+1} - \hat{\mathbf{w}}^n - \frac{\Delta_t}{2}\left(\Phi^T\mathbf{R}(\mathbf{W}_0 + \Phi\hat{\mathbf{w}}^n; \lambda)\right.$$
$$\left. + \Phi^T\mathbf{R}(\mathbf{W}_0 + \Phi\hat{\mathbf{w}}^{n+1}; \lambda)\right) = 0, \qquad (23)$$

where the superscript now denotes time level. At each time step, the nonlinear system (23) may again be solved with the chord method. For weakly nonlinear systems, the Jacobian $\mathbf{I} - \Delta_t\hat{\mathbf{J}}(\hat{\mathbf{w}})/2$ can be evaluated once at $t = 0$; with stronger nonlinearities the Jacobian can be periodically updated at additional computational expense.

Sensitivities of equilibrium solutions to α can be very efficiently predicted with POD-based ROMs. Three formulas are relevant: the relationship between full-system and ROM sensitivities, $\frac{d\mathbf{w}}{d\alpha} = \Phi\frac{d\hat{\mathbf{w}}}{d\alpha}$, the definition of ROM residuals, $\hat{\mathbf{R}} = \Phi^T\mathbf{R}$, and a condition on the ROM solution path

$$d\hat{\mathbf{R}} = \hat{\mathbf{J}}d\hat{\mathbf{w}} + \frac{\partial\hat{\mathbf{R}}}{\partial\alpha}d\alpha = 0, \qquad (24)$$

$$\frac{d\hat{\mathbf{w}}}{d\alpha} = -\hat{\mathbf{J}}^{-1}\frac{\partial\hat{\mathbf{R}}}{\partial\alpha}. \qquad (25)$$

From these formulas, it follows that sensitivities satisfy

$$\frac{d\mathbf{w}}{d\alpha} = \Phi\hat{\mathbf{J}}^{-1}\Phi^T\frac{\partial\mathbf{R}}{\partial\alpha}. \qquad (26)$$

The ROM is most beneficial for sensitivity analysis when there are several different parameters on which the system depends. In the procedure above, $\hat{\mathbf{J}}$ can be computed and decomposed once (as true for the steady-state analysis), and then repeatedly used in evaluating the sensitivity formula (26) for each variable. Following the decomposition of $\hat{\mathbf{J}}$, the primary computational expense in evaluating (26) is calculating $\frac{\partial\mathbf{R}}{\partial\alpha}$, which is variable dependent, but efficiently obtained.

The point at which (21) loses stability to time-oscillatory disturbances is a Hopf bifurcation point. The stability exchange occurs when a complex pair of eigenvalues of $\hat{\mathbf{J}}$ has vanishing real part, while other real components of the eigenvalues of $\hat{\mathbf{J}}$ are negative.[51] For small M, this process can be inexpensively and indirectly tracked through examination of all the eigenvalues of $\hat{\mathbf{J}}$. We define γ such that $\gamma(\alpha)$ is the real part of the eigenvalue of $\hat{\mathbf{J}}(\alpha)$ with largest real part; critical points of stability exchange, α^*, satisfy $\gamma(\alpha^*) = 0$. For practical problems, where M may not be very small, critical points can be directly found in a manner similar to that applied to aeroelastic systems by Beran and Morton.[70] The direct approach involves solving $\gamma = 0$ through Newton's method:

$$\left.\frac{\partial \gamma}{\partial \alpha}\right|_{\alpha = \alpha^\nu} \left(\Delta^{\nu+1}\alpha\right) = -\gamma(\alpha^\nu), \qquad (27)$$

where the correction $\Delta^{\nu+1}\alpha$ is typically relaxed with the parameter ω_{hopf}: $\alpha^{\nu+1} = \alpha^\nu + \omega_{\text{hopf}}\Delta^{\nu+1}\alpha$.

Nonlinear POD Formulation - Galerkin Projection

In comparison to the subspace projection method, a more compact and efficient ROM can be obtained through Galerkin projection. This approach is the most common technique used to obtain nonlinear ROMs through the proper orthogonal decomposition, including applications involving equations of fluid motion.[45, 46]

The projection procedure is derived from the original partial differential equations, written as

$$\frac{\partial \mathbf{w}}{\partial t} - \mathbf{R}(\mathbf{w}; \lambda) = 0, \qquad (28)$$

where $\mathbf{w}$ is now interpreted as a continuous field variable. As with the subspace projection method, the residual of (28) is forced to vanish after integrating the residual over the flow domain Ω, weighted by each POD mode $\mathbf{e}^k$ ($k = 1, 2, ..., M$):

$$\int_\Omega \mathbf{e}^k \left(\frac{\partial \mathbf{w}}{\partial t} - \mathbf{R}(\mathbf{w}; \lambda)\right) d\Omega = 0. \qquad (29)$$

The modes are obtained by: carrying out a numerical sampling process to obtain $\mathbf{S}$ in discrete form; solving a eigenvalue problem similar to (8); computing $\mathbf{\Phi} = \mathbf{SV}$, and scaling the modes to be orthonormal:

$$\int_\Omega \mathbf{S}^T \mathbf{SV} d\Omega = \mathbf{V\Lambda}, \qquad (30)$$

$$\int_\Omega \mathbf{e}^i \mathbf{e}^j d\Omega = \begin{cases} 1 \text{ if i = j} \\ 0 \text{ otherwise.} \end{cases} \qquad (31)$$

As an example, Park and Lee apply a Galerkin projection to the reduction of the Navier-Stokes equations in non-conservative form for the two-dimensional flow of an incompressible fluid.[45] They obtain a set of M

ordinary differential equations for $\hat{\mathbf{w}}$ following substitution of $\mathbf{w}(t) = \mathbf{\Phi}\hat{\mathbf{w}}(t)$ into the continuum equations (29) (for $k = 1, ..., M$):

$$\frac{d\hat{w}_k}{dt} = a_k + \sum_{l=1}^{M} \hat{w}_l P_{kl} + \sum_{l=1}^{M} \sum_{m=1}^{M} \hat{w}_l \hat{w}_m Q_{klm}, \qquad (32)$$

where a_k, P_{kl}, and Q_{klm} are elements of singly, doubly and triply indexed arrays computed by integrating over terms involving the M retained modes. For example, one term appearing in the expression for Q_{klm} is $\int_\Omega \mathbf{e}^k \mathbf{e}^l \frac{\partial \mathbf{e}^m}{\partial x} d\Omega$, which is evaluated numerically, since the modes are available in discrete form.

The main difference between the Galerkin and subspace projections is in the evaluation of spatial derivatives. With the Galerkin projection, modes are inserted into terms involving continuum derivatives that are integrated once in weighted fashion prior to numerical solution of the ROM. Alternatively, with the subspace projection, modes are dynamically inserted into the full, spatially discretized equations, which are then projected onto the ROM subspace. There are advantages and disadvantages associated with each approach. For the Galerkin projection, distillation of the original equations into a fully reduced-order system (e.g., (32)) yields a representation that can be very efficiently solved for steady and unsteady problems. However, the low computational cost of solving the ROM is accompanied by a high cost in the construction of the ROM. Returning to the Navier-Stokes equations for incompressible flow, the cost of computing the elements Q_{klm} is $\mathcal{O}(NM^3)$, which is impractical if M grows too large. Other potential drawbacks include: the need for ROM reconstruction if modes are changed; the lack of full-system data with which to assess model error; the need to have a problem-specific procedure by which ROMs are constructed, and the difficulty of expressing some parameters (e.g., those representing variations in local properties) in the ROM equations. The main disadvantage of the subspace projection method is evaluation of the full-system array $\mathbf{R}$ at each iteration, which increases the per iteration computational cost by at least $\mathcal{O}(N)$ and requires software linkage between the procedures that integrate the ROM and evaluate $\mathbf{R}$. However, this method is free from the drawbacks associated with the Galerkin projection method.

Nonlinear Dynamics with Harmonic Balance

The last technique to be described in this review is the harmonic balance (HB) formulation of Hall et al.[77] Their approach was first applied to the computation of time-periodic, nonlinear, viscous flows in 2-D turbomachinery cascades, and is now being used to analyze the aeroelastic behavior of airfoils in transonic flow.[78] The goal of the HB method is the efficient computation of time-periodic solutions of large, nonlinear systems.

Current methods based on time integration, for example those applied to aeroelastic computations,[79,80] can be very demanding owing to the need for retention of time accuracy. The requirement for small, global time steps and accurate integration over numerous cycles increases computational cost over steady-state analysis, for which large, local time steps can be used. With the HB method, the governing equations can be recast in a steady-state form that accounts for the underlying time periodicity of the solution, and which can be solved with pseudo-time-integration using standard acceleration techniques (local time stepping and multigrid acceleration).

There are several techniques, including harmonic balance, the finite-difference method, the shooting method, and the Poincaré map method, that have been applied to a large number of of relatively low-order problems involving nonlinear oscillations. These techniques are described in numerous texts and papers (and the references within).[81,82,83,84] The method of multiple scales has also been applied to the simulation of limit-cycle oscillation for an airfoil/flap configuration in transonic flow.[85]

However, the HB method developed by Hall et al. is designed to treat nonlinear, aerodynamic problems of practical size for which there are large shock motions.[77] To describe this technique, we choose $\mathbf{w}$ to be a discretized field variable with N degrees of freedom satisfying $\mathbf{w}(t) = \mathbf{w}(t + T)$, where T is the period of the oscillation. The solution is expanded in a Fourier series in time, truncated to $2N_{HB} + 1$ terms:

$$\mathbf{w}(t) = \sum_{n=-N_{HB}}^{N_{HB}} \mathbf{w}^n e^{j\omega nt}. \qquad (33)$$

The term $n = 0$ corresponds to the mean flow. Expansion (33) can be substituted into the governing equation (9) to obtain $2N_{HB} + 1$ equations for the vector coefficients in the Fourier expansion, $\mathbf{w}^n$, by collecting terms of like frequency. Using the nomenclature of Hall et al., these equations are written as $\tilde{\mathbf{S}}(\tilde{\mathbf{w}}) = \tilde{\mathbf{R}}(\tilde{\mathbf{w}}; \lambda)$, where in the unsteady term, $\tilde{\mathbf{S}}$ represents a collocation of the Fourier coefficients,

$$\tilde{\mathbf{S}} \equiv j\omega\tilde{\mathbf{N}}\tilde{\mathbf{w}}, \qquad (34)$$

$\tilde{\mathbf{R}}$ is a collection of nonlinear terms arising from the residual array, $\mathbf{R}$, $\tilde{\mathbf{N}}$ is a diagonal matrix containing the harmonic indices $(-N_{HB}, ..., 0, ..., N_{HB})$, and $\tilde{\mathbf{w}}$ is the set of vector coefficients

$$\tilde{\mathbf{w}} = (\mathbf{w}^{-N_{HB}}, ..., \mathbf{w}^0, ..., \mathbf{w}^{N_{HB}})^T. \qquad (35)$$

The evaluation of $\tilde{\mathbf{R}}$, what Hall et al. call the harmonic fluxes, is computationally expensive $(\mathcal{O}(NN_{HB}^3))$ for the Euler equations and not easily extended to turbulent, viscous flows.[77] They propose an alternative harmonic balance formulation that is

both simpler and more efficient. First, $\mathbf{w}$ is defined at $2N_{HB} + 1$ instants in time, evenly distributed about the periodic orbit, and collected into a single array $\mathbf{w}^*$:

$$\mathbf{w}^* = \left(\mathbf{w}(0), \mathbf{w}\left(\frac{T}{2N_{HB} + 1}\right), ..., \mathbf{w}\left(\frac{2N_{HB}T}{2N_{HB} + 1}\right)\right).$$

Then, the discrete Fourier transform operator, $\tilde{\mathbf{E}}$, which is an $NN_{HB} \times NN_{HB}$ blocked matrix, is used to relate $\mathbf{w}^*$ and $\tilde{\mathbf{w}}$ according to $\tilde{\mathbf{w}} = \tilde{\mathbf{E}}\mathbf{w}^*$. Substitution of this expression into the equation $\tilde{\mathbf{S}} = j\omega\tilde{\mathbf{N}}\tilde{\mathbf{w}} = \tilde{\mathbf{R}}$ provides

$$j\omega\tilde{\mathbf{E}}^{-1}\tilde{\mathbf{N}}\tilde{\mathbf{E}}\mathbf{w}^* = \mathbf{R}^*, \qquad (36)$$

where $\mathbf{R}^*$ is the residual array evaluated at the $2N_{HB} + 1$ temporal points. The right-hand side of (36) reduces to a simple form, since when the governing equations are in strong-conservation form, the product $\tilde{\mathbf{E}}^{-1}\tilde{\mathbf{E}} = \tilde{\mathbf{I}}$ can be formed through the linear derivative expressions in $\mathbf{R}$.

Finally, Hall et al. introduce a pseudo-time τ^{77} by which (36) is integrated towards "steady state:"

$$\frac{\partial \mathbf{w}^*}{\partial \tau} + j\omega\tilde{\mathbf{E}}^{-1}\tilde{\mathbf{N}}\tilde{\mathbf{E}}\mathbf{w}^* = \mathbf{R}^*(\mathbf{w}^*; \lambda). \qquad (37)$$

This step is an important benefit of the HB method, because it allows the time-dependent solution to be computed with existing, accelerated steady-state methods that need far fewer iterations than time-accurate, time-integration methods. In this formulation, the "unsteady" term is replaced by $j\omega\tilde{\mathbf{E}}^{-1}\tilde{\mathbf{N}}\tilde{\mathbf{E}}\mathbf{w}^*$, requiring $\mathcal{O}(NN_{HB}^2)$ operations to evaluate (e.g., the multiplication of $\tilde{\mathbf{E}}\mathbf{w}^*$), an improvement over the HB method in fully spectral form. Furthermore, Hall et al. report that the evaluation of the fluxes, $\mathbf{R}^*$, which requires $\mathcal{O}(NN_{HB})$ operations using standard techniques, dominates the cost of the numerical scheme.[77]

We comment that the HB technique does not involve a reduction in the number of variables arising from spatial discretization, and does not provide a model that is a compact representation of the full system. However, this technique does yield an efficient and low-order representation of the temporal variations of complex systems experiencing cyclic behavior in time. Also, a form of this HB method that allows the period T to be explicitly treated as an unknown (i.e., for an autonomous system) is currently being developed by Hall and his colleagues.

Results

In this section, we present results obtained with the Volterra theory of nonlinear systems and the proper orthogonal decomposition. Attention is primarily restricted to problems in unsteady aerodynamics and aeroelasticity, but results in other fields are drawn upon to show the wide applicability of the techniques. Volterra first-order kernals are used to simulate the
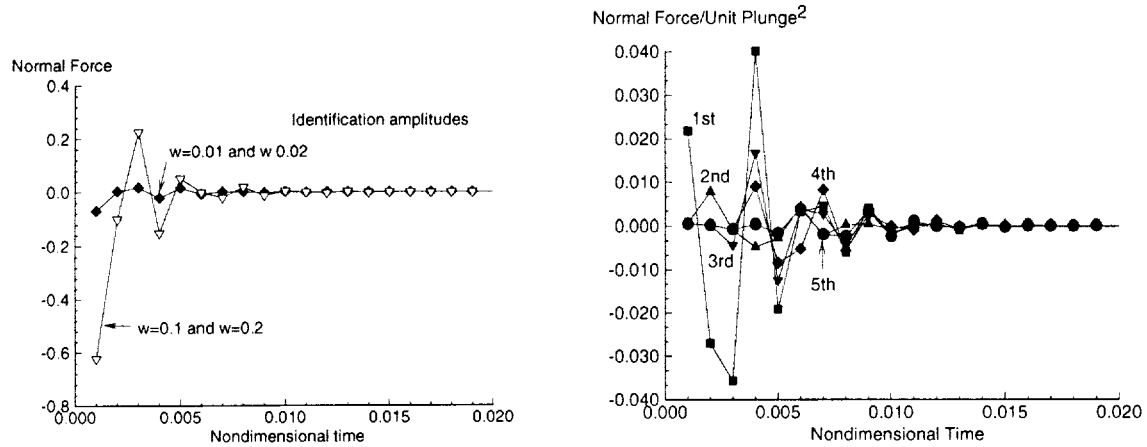
Fig. 1 Volterra kernels for CFD analysis of RAE airfoil. Left: first-order kernel and effect of ID amplitudes. Right: First five components of the second-order kernel for plunge.

unsteady response of viscous flows about driven airfoils, and the aeroelastic response of airfoils and wings. Higher accuracy can be achieved with second-order kernals, and the relative improvement is quantified for selected configurations. We also report on Duke University's application of POD to the rapid prediction of flutter boundaries of airfoils and wings in the transonic regime[50,55] and Air Force Research Laboratory's investigation of reduced-order forms of the discrete Euler equations.[52,54] The section is concluded with a summary of results obtained with the harmonic balance technique of Hall et al.[77]

Volterra Series Analysis

First- and second-order kernels for the Navier-Stokes solution (with Spalart-Allmaras turbulence model) of an RAE airfoil in plunge at a transonic Mach number using the CFL3D code[86] are presented in Fig. 1. On the left are two sets of first-order kernels due to two different sets of excitation amplitudes. Recall that the first-order kernel is computed using (3) and is the result of two pulse responses, one at a particular amplitude and the second at double the first amplitude. One of the first-order kernels shown in Fig. 1 was computed using excitation plunge amplitudes of $w = 0.01$ and $w = 0.02$, where w is a percent of the chord of the airfoil. The other first-order kernel was computed using excitation plunge amplitudes of $w = 0.1$ and $w = 0.2$. It is clear that the two kernels are not linearly related, demonstrating how the first-order kernel can capture amplitude-dependent nonlinear effects. On the right of Fig. 1 are five components of the second-order kernel for this case. The second-order kernel is more complicated because it is a two-dimensional function of time. The important point to be made is that this kernel is readily generated and its relatively smaller values (compared with the first-order kernel) and its rapid convergence indicate a small (but not negligible) level of nonlinearity present. This information might

be used to determine that the first-order kernel may be sufficient to capture the dominant nonlinear effects. This point is demonstrated in Fig. 2

Fig. 2 is a comparison of plunge responses for three different plunge amplitudes for the same configuration. Specifically, a comparison is made between the full CFD solution due to a sinusoidal plunging motion and that obtained using the first-order kernel from Fig. 1 (due to the larger excitation amplitudes). As can be seen, the plunge response obtained using the Volterra first-order kernel compares identically with the response obtained from the full CFD solution for the two smaller amplitude responses. The comparison for the largest amplitude response (i.e., nonlinear) is very good as well, with a slight but noticeable difference between the two results. The nonlinearity of the large- amplitude plunge responses is confirmed by linearly scaling the smallest amplitude (i.e., linear) response which, as shown in Fig. 2, cannot capture the amplitude-dependent nonlinear plunge dynamics seen at the larger amplitude. The turnaround time ("wall-clock") for the full CFD solution was on the order of a day whereas the Volterra first-order solution was computed on a workstation in 30 seconds using digital convolution. The initial cost of computing the first-order kernel was trivial as well due to the rapid convergence of the pulse responses. In fact, since each pulse (unit and double amplitudes) goes to zero in less than 100 time steps, the responses were generated using a debugging mode option available on the supercomputer system used. Using this option, computations requiring less than 300 time steps are executed immediately, intended for debugging purposes. As a result, each pulse was computed within five minutes, resulting in a first-order kernel that was computed in about ten minutes. Of course, once the kernel has been computed, it can be used to predict the response to an arbitrary input (steady, any and all frequencies, random) of arbitrary length via digital convolution on a

workstation. Using this method, there is no need for the repeated, and costly, execution of the CFD code for different inputs.
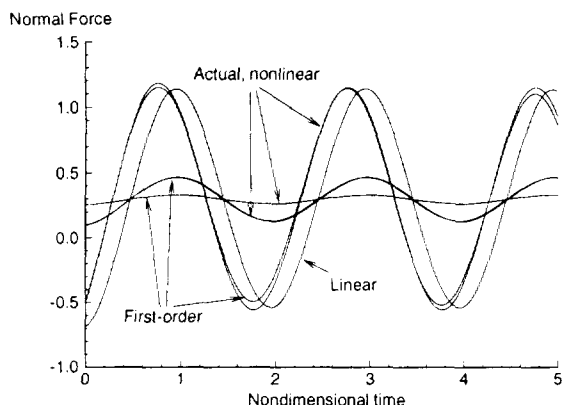

Fig. 2 Comparison of actual nonlinear and first-order Volterra responses for three different plunge motions and a linear response for the largest motion.

Raveh, Levy and Karpel have recently applied the Volterra-based ROM approach to analysis of the AGARD 445.6 wing.[14] They simulate the flow field around the wing using the EZNSS Euler/Navier-Stokes code.[87] This code provides a choice between two implicit algorithms, the Beam-Warming algorithm and the partially flux-vector splitting algorithm of Steger et al. Grid generation and inter-grid connectivity are handled using the Chimera approach. The code was enhanced with an elastic capability to compute trimmed maneuvers of elastic aircraft.[87] For the CFD computations, the flow field around the wing was evaluated on a C-H type grid, with 193 points in the chordwise direction along the wing and its wake, 65 grid points in the spanwise direction, and 41 grid points along the normal direction.

A process of mode-by-mode excitation, discussed previously, was performed for this wing using four elastic modes at a Mach number of 0.96. The mode-by-mode excitation technique provides the unsteady aerodynamic response in all four modes due to an excitation of one of the modes. In this fashion, a matrix of four-by-four functions (sixteen total) is developed. Two sets of excitation inputs were used: the discrete-time pulse input and the discrete-time step input. The cost of computing these functions is minimal due to the rapid convergence of these functions and it consists of only four code executions. Once these functions were defined, several full CFD solutions were generated that were due to various sinusoidal inputs at various frequencies. Shown in Fig. 3 is just one of these results for a 5 Hz input frequency, comparing the result obtained from the full CFD solution to that obtained via convolution of the step or pulse responses with a 5 Hz sinusoid. As can be seen, the comparison is

exact to plotting accuracy for most of the responses. The full CFD solution, consisting of 8000 iterations required approximately 24 hours on an SGI Origin 2000 computer with 4 CPUs. By comparison, the Volterra-based ROM response shown required about a minute. Even including the upfront cost of computing the pulse (or step responses), the computational cost savings are significant. More importantly, the same pulse (or step) functions can now be used to predict the response of the aeroelastic system to any arbitrary input of any length.

Shown in the left and middle portions of Fig. 4 is a comparison of linear and nonlinear GAFs for the first two modes of the AGARD 445.6 Aeroelastic Wing at a Mach number of 0.96. Nonlinear GAFs refers to the GAFs computed using the Volterra pulse-response technique about a nonlinear steady-state value by exciting one mode at a time and obtaining the resultant responses in the other modes. The CFD results are compared with those using the ZAERO code for a purely linear case. Frequency-domain values were obtained by performing a convolution of several frequencies of interest with the computed CFD-based pulse responses. As can be seen, the comparison is reasonable and shows the small (but not negligible) nonlinear aerodynamic effects identified using the Volterra pulse-response technique.

But rather than transforming the time-domain GAFs into the frequency domain, discrete-time, state-space systems can be created using the Volterra pulse responses directly. Presented in the right portion of Fig. 4 is a comparison of the pulse responses for the AGARD 445.6 Aeroelastic Wing due to a unit pulse in the first mode. The CFD-based pulses (circles) compare exactly with the pulse responses obtained from a state-space system generated to model this system. The 32nd-order state-space system is a complete representation of the entire frequency spectrum of the unsteady aerodynamics defined by the GAF influence functions for the four aeroelastic modes of this wing. The pulse responses due to unit pulses in the second, third, and fourth mode are just as good as those shown in Fig. 4, but are not presented here for brevity.

POD Analysis

The proper orthogonal decomposition has been applied to a variety of multidisciplinary problems involving the aerodynamic equations. In the remainder of the Results section, we summarize recent findings arising from the reduction of system order through POD-based modeling. We first review application of the frequency-domain POD to aeroelastic systems in two and three space dimensions, and then describe progress in the analysis of nonlinear equation sets with POD, including those that exhibit limit-cycle oscillation. This section closes with a summary of stability results obtained for a front-stage rotor in viscous flow
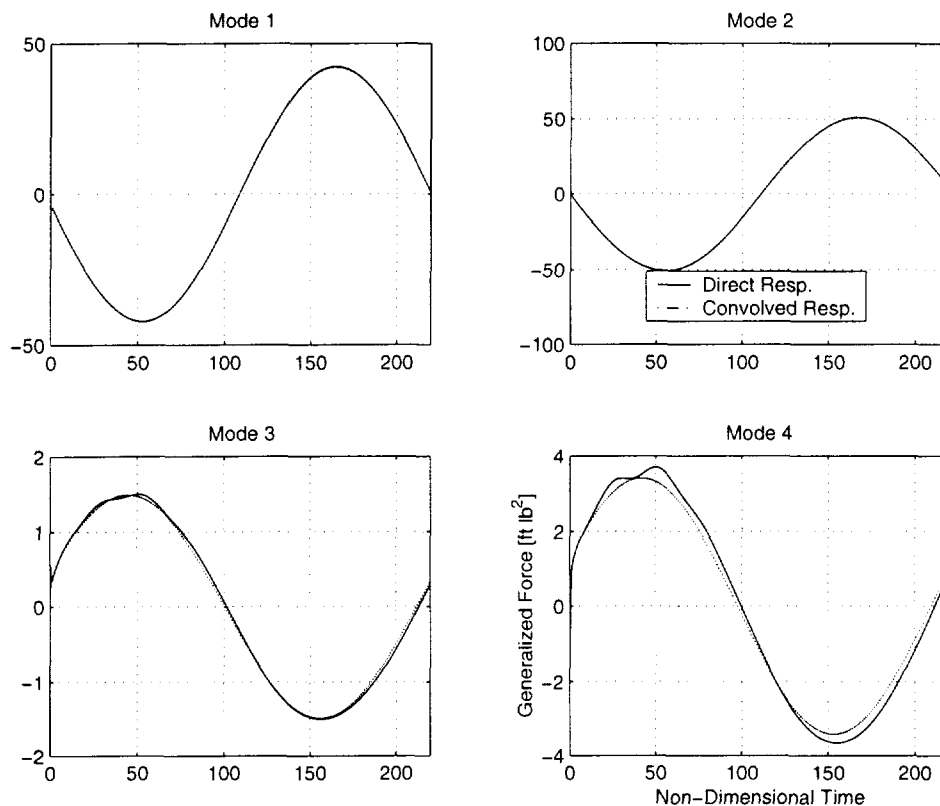
Fig. 3   Comparison of direct and convolved responses to sinusoidal excitation at 5 Hz (Mach 0.96).

using the harmonic balance technique.

Linear (Frequency Domain) POD Analysis

Hall, Thomas and Dowell[50] report an application of their linear POD formulation to a two-dimensional aeroelastic configuration, and, in an ongoing study, Thomas, Dowell and Hall[73] extend this previous work to the analysis of three-dimensional wings. In 2-D, Hall et al. develop POD-based ROMs for the NASA Ames Research Center NACA 64A010 airfoil with a pitch and plunge structural model representative of a swept-wing section.[88] Base solutions of the Euler equations, W_0, are computed with a node-centered Lax-Wendroff scheme for freestream Mach numbers, M_∞, between 0.7 and 1.0. A shock first becomes evident in the base flow solution near the airfoil crest at about Mach 0.8. The aerodynamic equations are solved on grids of O topology; solution insensitivity to grid refinement is verified using a sequence of grids involving 65 × 33, 97 × 49 and 129 × 65 nodes.

Reduced-order models of the flow equations are constructed from solution snapshots resulting from two independent airfoil movements about base states: pitch oscillation and plunge oscillation. Using the procedure detailed in the Analysis section, snapshots are computed from (15) for reduced frequencies (nondimensionalized by freestream velocity and airfoil chord) evenly distributed between -1 and 1. Following collection of 41 snapshots, Hall et al. assemble ROMs with

up to 41 retained modes.[50] A ROM is computed for each different Mach number (and base flow) examined. The aerodynamic equations in reduced-order form are then coupled with the structural equations, leading to the low-order, aeroelastic eigenproblem (19).

Hall et al.[50] carry out very efficient analyses of (19) to construct flutter boundaries for the thickened NACA 64A010 airfoil. Their results are summarized in Fig. 5. Flutter speeds predicted with POD-based ROMs compare well with those previously reported from transonic small-disturbance analyses,[88,89,90] and are used to document precisely the fold in the flutter boundary characteristic of the NACA 64A010 airfoil. As observed by Hall et al., the Mach number at which the fold occurs is underpredicted by the small-disturbance analyses relative to the POD-based Euler analysis.[50] Fig. 5 also illustrates that the POD results are well converged in the number of grid points used in the CFD computations and the number of modes retained in the ROM. For only a small set of Mach numbers do the results obtained with either the coarsest grid or the fewest number of retained modes deviate from the remaining results. In particular, the highly nonlinear behavior around Mach 0.9 is well defined in most cases.

In work soon to be published,[73] Thomas et al. have extended the linear POD formulation to the analysis of the (weakened) AGARD 445.6 wing. Their in-
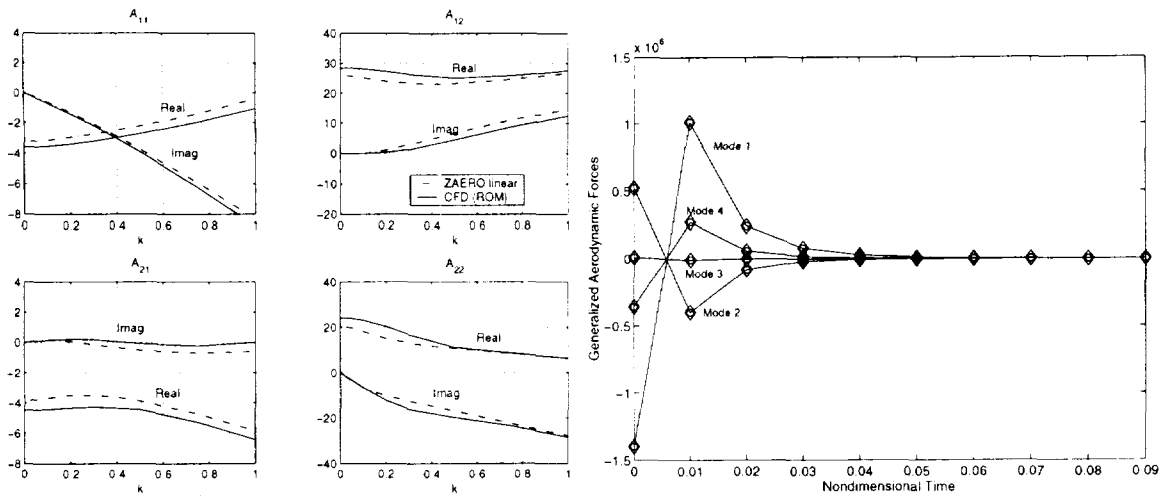
Fig. 4 Volterra results for the AGARD 445.6 wing at Mach 0.96. Left and Middle: Comparison of linear and nonlinear GAFs for the first two wing modes. Right: Comparison of pulse responses.
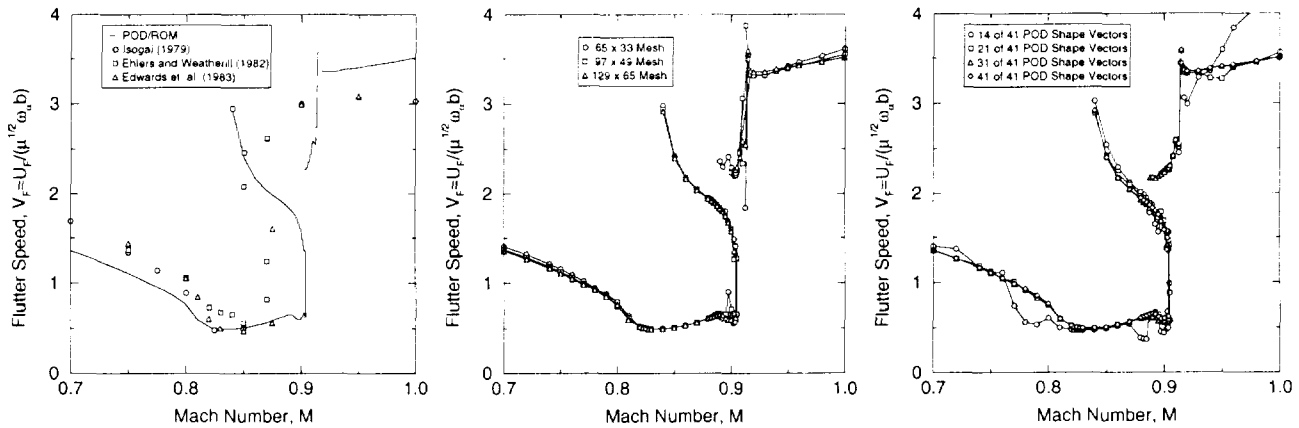

Fig. 5 Flutter speed of NASA Ames Research Center NACA 64A010 airfoil for various Mach numbers computed with frequency domain, POD-based ROMs. Left: results from 41-mode ROM (finest grid) versus other computational results; Middle: sensitivity of 41-mode ROM to grid refinement; Right: sensitivity of POD results (finest grid) to number of retained modes (from Hall et al.[50] with permission).

vestigation addresses two potential concerns for the application of POD-based methods to practical aeroelastic configurations: the size of ROMs necessary to capture 3-D effects, and the sampling requirements associated with a multiplicity of configuration-dependent structural modes. Thomas et al. compute base flow solutions of the Euler equations with a grid of O-O topology containing $49 \times 33 \times 33$ nodes, and construct flutter boundaries through POD analysis for Mach numbers between 0.5 and 1.141. They develop POD-based ROMs using two approaches. First, a 55-mode POD is built at each Mach number by computing solutions of (15) at reduced frequencies evenly distributed between 0 and 0.5 (conjugate solutions are associated with negative frequencies) for the first 5 natural modes of the wing structure. With this surprisingly small number of POD modes, Thomas et al. obtain results that are very consistent, in terms of flutter speed and

frequency ratio, with those published by Lee-Rausch and Batina.[91] Thomas et al. also propose and demonstrate a promising technique for reducing the number of snapshots necessary to construct an effective POD-based ROM for an aeroelastic configuration. With this approach, only two snapshots are required for each natural mode of the structure, in addition to a set of "fundamental" modes, to construct the aeroelastic ROM.

Nonlinear POD Analysis - Subspace Projection

To study the application of POD to problems in aeroelasticity for which the reduced-order model is nonlinear, Pettit and Beran have first examined flowfield response to steady and unsteady changes in structural shape. One such problem which has proved valuable is the response of inviscid flow over a deforming panel in two space dimensions.[52,75] The flowfield

is situated above an infinite, panel that lies in the $y = 0$ coordinate plane, except for a segment between $x = -\frac{1}{2}$ and $x = \frac{1}{2}$ for which the panel shape is a parabolic arc defined by $y_s(x,t) = \delta(t)\left(1 - 4x^2\right)$. For steady problems, the amplitude parameter δ is a specified constant, while for unsteady problems, $\delta(t) = \delta_1 \sin(\omega t)\left(1 - e^{-\alpha t}\right)$ is assumed, where δ_1, ω, and α are constants. The length of the "bump" and the far-field velocity, U_∞, serve in the nondimensionalization of the aerodynamic analysis. A schematic of the bump and the 71 × 141 baseline grid are shown in Fig. 6. The flowfield response is assumed to be gov-
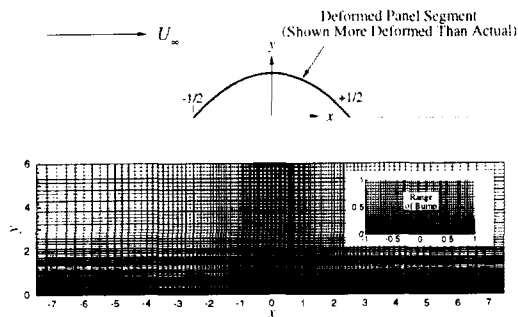
Fig. 6 Top: Schematic of panel and coordinate system. Bottom: Baseline grid.

erned by the Euler equations, which are discretized and solved with the upwind total variation diminishing scheme of Harten-Yee.[92,93] A transpiration condition is used by Pettit and Beran to satisfy approximately the boundary conditions on the bump surface while not requiring grid deformation.

Pettit and Beran[53] conduct an analysis of flow changes in response to static changes in amplitude of the bump described above, and their preliminary results are summarized here. The algorithm for full-system analysis is validated by comparing computed results with those obtained using Cobalt$_{60}$, an unstructured, finite-volume algorithm for the Euler and Navier-Stokes equations[94] that has been validated extensively. Differences in the predictions of the two techniques are small for variations of both Mach number and bump amplitude in the range of interest.

A single, reduced-order model for the steady-state bump is constructed from 26 full-system solutions computed at Mach 1.1, 1.15, 1.2, 1.25 and 1.3. At each Mach number, snapshots are computed at several different values of δ. For a given Mach number, there is a critical bump amplitude beyond which the shock attached to the leading edge of the bump detached, forming a bow shock. At sufficiently large values of δ and prior to shock detachment, response of the system is nonlinear to changes in δ. Once the bow shock forms, flow structure (i.e., shock position) becomes highly sensitive to additional changes in Mach number and bump amplitude, a situation not well suited

for POD analysis. Thus, most sampling and ROM application is limited to cases for which the flow is entirely supersonic.

With 26 solutions, a total of 104 modes are computed. Pettit and Beran examine results when all modes are included in the analysis and when there is truncation to 60 and 40 modes.[53] Full-system solutions of (9) are time integrated to steady-state with 2000-10000 function evaluations, depending on parameter selection, and are initialized with uniform flow. While these cases were computed serially, they could also have been computed in parallel. Up to a point, sampling is a naturally parallel process; as a solution space is revealed, fill-in cases can be computed when resources become available. Equilibrium solutions of the POD-based ROM, satisfying (22), are computed along paths of constant Mach number and varying δ, starting with the trivial solution at $\delta = 0$ and progressing in increments of $\Delta_\delta = 0.001$. At each point, ROM values are initialized using the previous solution, and solutions are typically computed in 3-10 function evaluations. Computing on the order of 100 solution points with the ROM typically requires fewer function evaluations than that necessary for a single solution of the full-system.

Pettit and Beran interpreted the steady-state results using the minimum local Mach number, which typically is observed at the bump leading edge.[53] Examination of other flow variables did not alter their conclusions concerning the viability of the POD-based ROM. Solutions are compared in Fig. 7. Full-system solutions not used as ROM snapshots are also computed to obtain predictions of system behavior away from snapshot locations. Norms of the full-system residual are readily computed after each function evaluation in the subspace projection method and used to evaluate the quality of reduced-order solutions. Modeling of parameter-space subdomains where residual norms become unacceptably high can be improved by retaining different sets of modes or through model reconstruction. In the figures just cited, only ROM solutions with a residual norm less than 0.6 are displayed. Pettit and Beran found this cutoff value to be consistent with good ROM solutions for the configuration being investigated. When 60 or all 104 modes are retained, ROM solutions are highly accurate and reproduce the nonlinear behavior evident in the response of the full system. Interestingly, the 60-mode ROM is somewhat superior to that of the full, or 104-mode, ROM. Pettit and Beran speculate that higher order modes in the 104-mode ROM, which possess length scales on the order of the node spacing, can lightly pollute solutions with the present scheme, which makes no attempt to filter out such modes. However, in the steady-state analysis, modes are retained that are much smaller in magnitude (eigenvalues of $\mathbf{S}^T\mathbf{S}$ as small as 10^{-10}) than that of the dynamic analysis. The fundamental diffi-

culty with retaining low-energy modes in the dynamic analysis is not observed in the steady-state analysis. This is not a practical problem, since it is desirable to use fewer than the maximum number of modes. When the number of retained modes is decreased to 40, the accuracy of the ROM is nominally degraded, and the number of computed points satisfying the residual norm cutoff is diminished. Most notably, solutions at Mach 1.1 do not meet this criterion, which may not be surprising, since these points are on the boundary of the snapshot region and reflect the most nonlinear fluid dynamic behavior.

Beran and Pettit have also computed unsteady solutions of the Euler equations for supersonic flow over an oscillating bump with an implicit, POD formulation. Their results were recently presented at the ICES '2K Conference,[75] and are reported here to document the robustness and accuracy of the implicit technique described in the Analysis section. They consider a Mach 1.2 flow over a bump with oscillation specified by the following baseline parameters: $\delta_1 = 0.005$, $\omega = 1.0$, and $\alpha = 3$. The computational domain is discretized in a manner equivalent to that used in the steady-state analysis. A POD-based ROM is constructed for the baseline case by explicitly integrating the discrete equations, expressed as (9), and collecting snapshots. Integration is carried out for 20 time units (approximately 4 cycles) with a time step of 0.01, the maximum value observed to permit stable integration. A total of 200 snapshots, each representing a collocation of the conserved variables over the computational domain, are collected at 10-iterate intervals. The initial state of the flowfield is specified to be uniform flow at freestream conditions and is used in the definition of $\mathbf{W}_0$.

Pettit and Beran[52] block the snapshot matrix so that the non-trivial elements of each column of $\mathbf{S}$ represent only one of the conserved variables at a specified instant. In this manner, the 200 snapshots described above fill $\mathbf{S}$, which is organized as a block diagonal matrix with a total of 800 columns. Each block is associated with one of the conserved variables, as are each of the 800 computed modes. This approach is inefficient for very large problems owing to the increased size of $\mathbf{S}$, but leads to an adaptable framework for computing modes for each conserved variable.

Following (8), ROMs are computed for between 6 and 20 retained modes. With 20 modes retained, the number of degrees of freedom is decreased by a factor of 2000. Pettit and Beran observe that with as few as 8 modes retained, ROM integration yields very accurate results in comparison to full-system analysis for the case used to construct the reduced-order model. This is illustrated qualitatively in the left and middle portions of Fig. 8, where the structure (and magnitudes) of the density fields near the bump explicitly computed with a 14-mode ROM and full-system

analysis are nearly identical (shown at the end of the sampling period, $t = 20$). In the right portion of Fig. 8, time histories of pressure at the bump midpoint are reported for a 10-mode ROM implicitly computed with the Crank-Nicolson scheme. There it is seen that implicit integration of the ROM accurately reconstructs the aerodynamic response, even using time steps 40 times larger than needed for explicit integration of the full system. Results are shown for 5 subiterates in the Crank-Nicolson scheme; solutions can be obtained with 2 subiterates (without loss of accuracy) an order-of-magnitude faster than with full-system analysis.

In a manner motivated by the frequency-domain analysis of Hall et al.,[50] Pettit and Beran,[53] construct hybrid ROMs combining snapshots computed for different bump amplitudes and frequencies. These hybrid ROMs successfully reproduce aerodynamic responses for cases not explictly included in the sampling process. Pettit and Beran also report[52,53] for the bump problem that the subspace projection method yields numerically divergent results when the number of retained modes exceeds 19. By increasing the number of modes, the onset of divergence can be delayed, and the accuracy of the ROM solution increased prior to divergence. At present, the cause of this instability has not been identified; however, a violation of mass conservation in the system can be associated with the onset of divergence, which suggests a direction for future examination.

Nonlinear POD Analysis of Limit-Cycle Oscillation

To assess the applicability of POD-based ROMs to differential equations that exhibit limit-cycle oscillation (LCO), Beran et al.[51] computed solutions of a tubular reactor, known to experience LCO,[95,96] with the subspace projection technique. The governing equations are

$$\frac{\partial w_1}{\partial t} = Lw_1 - w_1 Q(w_2), \qquad (38)$$

$$\frac{\partial w_2}{\partial t} = Lw_2 - \beta_1 (w_2 - \beta_3) + \beta_2 w_1 Q(w_2), \qquad (39)$$

$$L \equiv \frac{1}{\text{Pe}} \frac{\partial^2}{\partial x^2} - \frac{\partial}{\partial x}, \qquad Q(w_2) = \mu \exp\left(\Gamma - \frac{\Gamma}{w_2}\right),$$

where Pe, β_1, β_2, β_3, Γ, and μ are specified parameters. Equations (38) and (39) describe convection, diffusion and reaction within the reactor, and are referred to as the CDR equations. The variables w_1 and w_2 represent concentration and temperature, respectively, and the parameter μ (the Damkohler number) determines the ability of the CDR equations to sustain LCO. The spatial domain is normalized; boundary conditions are applied at $x = 0$ and $x = 1$. Following spatial discretization of the equations and specification of suitable initial conditions, which are details described elsewhere,[51] the CDR equations take the form $\frac{d\mathbf{w}}{dt} = \mathbf{R}(\mathbf{w}; \mu)$.
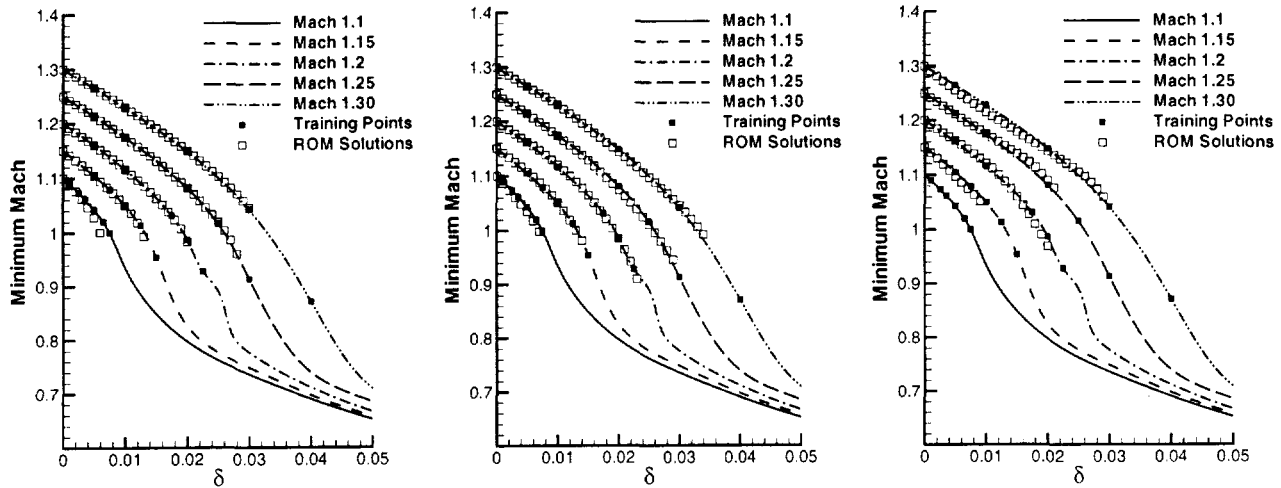
Fig. 7 Minimum local Mach number achieved by full-system and ROM solutions at selected freestream Mach numbers and bump amplitudes: Left: All 104 modes; Middle: 60 modes; Right: 40 modes.
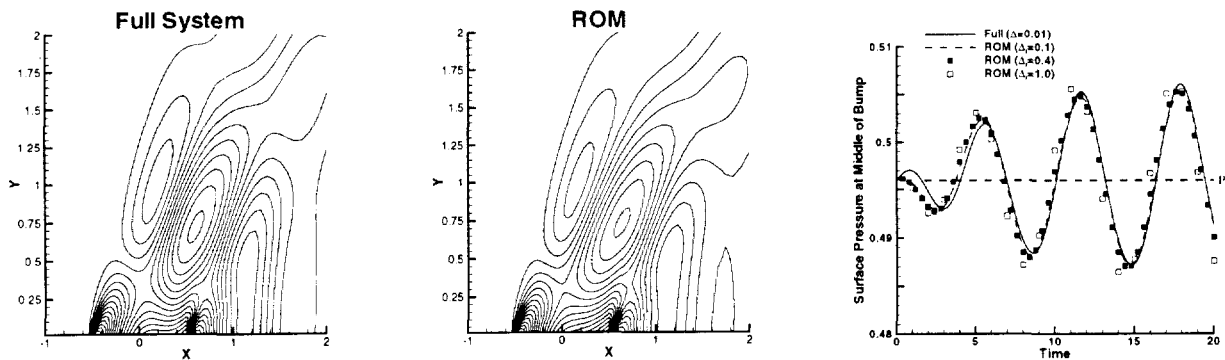

Fig. 8 Comparison of full-system and POD-based ROM predictions of aerodynamic response to bump oscillation ($\delta_1 = 0.005$). Left and Middle: Computed density contours at time $t = 20$ (14-mode ROM). Right: Time histories of computed surface pressure at bump midpoint for different integrations of 10-mode ROM.

The CDR system experiences a supercritical Hopf bifurcation at $\mu^* = \mu = 0.16504$,[51] which is accurately predicted by a POD-based ROM. The stability properties of the CDR system are shown in Fig. 9, where it is seen that stability of the equilibrium system is lost beyond the bifurcation point. Solutions are characterized by the maximum value of temperature computed over the domain, T_{max}. The ROM is developed by sampling the CDR system as it evolves towards steady-state ($0 \leq t \leq 2.5$) for a value of μ leading to system stability: $\mu^0 = 0.16 < \mu^*$. Following the procedure described above, 8 modes are computed and retained, representing a 15-fold reduction in problem size. Solutions of the full system are explicitly computed with time integration using a maximum time step of 0.0005 (limited by numerical stability). Equilibrium solutions of the ROM are computed with the

procedure described above, while LCO solutions are found with an explicit procedure like that applied to the full system.[51] It should be noted that even with the explicit procedure, dynamic solutions of the ROM can be obtained with time steps 50 times larger than 0.0005. This increase in allowable time step is a consequence of the absence of high-frequency, odd-even modes in the POD-based ROM that would destabilize the numerical scheme.[51]

Equilibrium solutions of the full system and the ROM are observed to be in excellent agreement. As seen in Fig. 9 (left), agreement is nearly exact at $\mu^0 = 0.16$, where the POD is constructed, and is excellent for the remaining values of μ shown. A slight inaccuracy is introduced at the Hopf point, where new system behavior becomes available. Beyond the Hopf point, LCO amplitude is well predicted with the ROM.
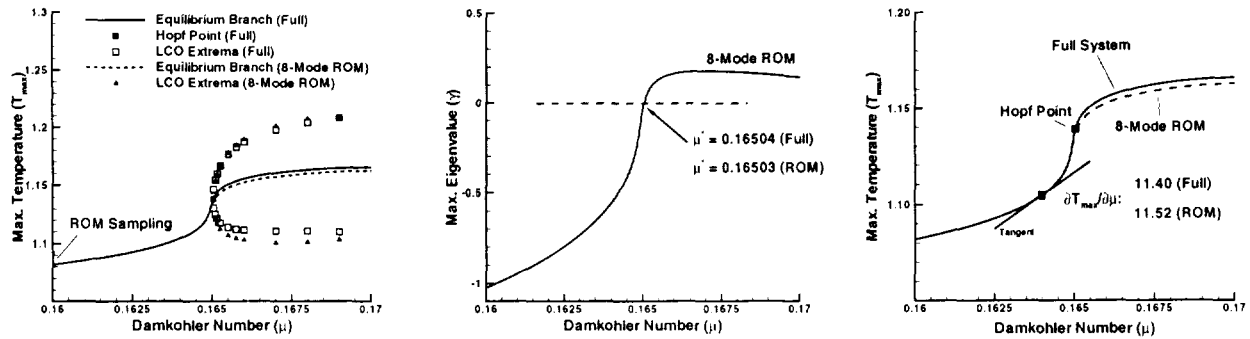
Fig. 9 Comparison of full-system and ROM solutions for an 8-mode ROM trained at $\mu^0 = 0.16$. Left: Equilibrium and LCO branches. Middle: ROM system stability. Right: Sensitivity to μ variation.

Quantitative differences between ROM and full-sytem solutions can be reduced with nominal improvements in sampling (increasing the number of retained modes or increasing the sampling period).[51]

The critical value of μ at which the CDR system loses stability is also very accurately predicted using reduced-order modeling. The variation of the stability parameter γ computed with the ROM (cf. (27)) is shown in Fig. 9 (middle). Stability loss is observed at $\mu = 0.16503$, nearly the same value predicted with the full-system equations ($\mu = 0.16504$). The Hopf point is computed directly with Newton's method in 11 iterations ($\omega_{\text{hopf}} = 0.5$), starting with the equilibrium solution at $\mu = 0.16$.

Sensitivity of the variable T_{max} to the bifurcation parameter μ is computed with the ROM formulation (26) at $\alpha = 0.164$ using the 8-mode ROM described above. As shown graphically and quantitatively in Fig. 9, the accuracy is excellent, with only a 1% difference between the ROM and full-system results.

Nonlinear POD Formulation with Shocks

The application of POD to flows with shocks is a challenging endeavor, owing to the obvious difficulty of capturing movements of solution discontinuities with a fixed set of global modes. In preliminary work, the utility of ROM/POD for modeling the quasi-static movement of strong shock waves in a quasi-one-dimensional nozzle, assuming inviscid flow, is being assessed.[97] The location of the standing shock is varied by altering the the boundary conditions and/or the ratio of specific heats. It is observed that with straight-forward application of the nonlinear POD analysis described above, accurate modeling of shock movement requires an excessively large number of modes and data samples. Essentially, one snapshot is needed for every grid point location traversed by the moving shock.

To improve the effectiveness of POD for problems of this type, a domain decomposition approach has been successfully developed as part of an ongoing investigation.[97] In this approach, regions of the flow field

that do not experience shocks are modeled with POD, while the flow-field region over which the shock moves, identified during the sampling procedure, is modeled with the full-system equations. See Fig. 10. With almost no degradation of accuracy, this methodology captures shock movement in the nozzle using an order-of-magnitude fewer degrees of freedom. An extension of these techniques is currently underway for a two-dimensional configuration where greater levels of order reduction are anticipated.
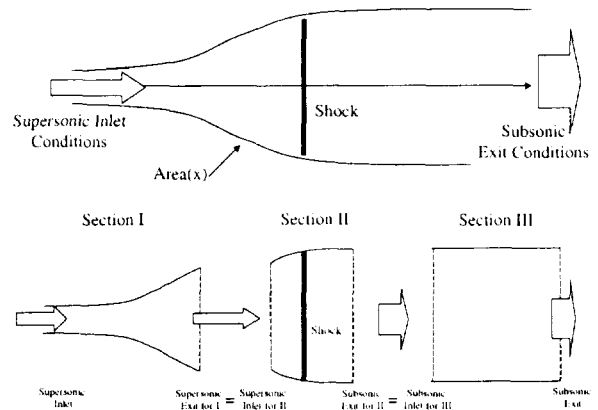

Fig. 10 Top: Nozzle with standing shock. Bottom: Decomposed domain for POD analysis.

Nonlinear POD Analysis - Galerkin Projection

Galerkin projection is being used by a number of investigators to develop POD-based ROMs of low order for the study of various nonlinear phenomena. One noteworthy example is the work of Cizmas (Texas A&M University) and Palacios (San Diego State University), which involves the construction of reduced order models for two-phase flow, heat transfer and combustion in dense or dilute fluid-solids flows. Their ongoing research project has several objectives: numerical generation of a database that includes spatio-temporal samples of system variables; modal decompo-
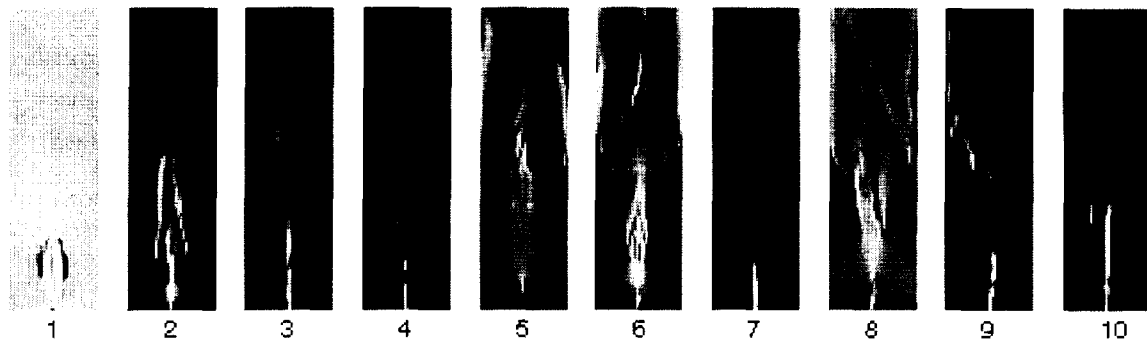
Fig. 11 Snapshots of gas velocity in the y-coordinate direction at 10 equally spaced time instants of a gas/solid mixture.

sition of these variables through POD analysis; identification and separation of dominant spatial structures during the evolution of the fluid and solids phases; Galerkin projection of the governing partial differential equations onto POD-basis functions to produce a low-dimensional set of ordinary differential equations, and development of visualization tools for low-order models.

Preliminary results obtained by Cizmas and Palacios demonstrate the ability of the POD to capture efficiently the energy content in a gas/solid mixture. The 2-D configuration is jet flow into a fluidized bed (40cm × 60cm) of 500 micron particles. The governing transport equations are much more complex than the Navier-Stokes equations; 3 gas and 3 solids equations comprise the set. Illustrated in Fig. 11 are ten snapshots of the y-component of velocity taken at equal intervals in time that partially represent the ensemble of snapshots over all system variables. The snapshots are used in the computation of 20 POD modes for this component of velocity that account for 80% of the system energy (ratio of sum of retained POD eigenvalues to sum of all POD eigenvalues). Flow asymmetries about the vertical axis are captured in several retained modes. Their ongoing work, which is yielding promising results, is now focused on computing a low-dimensional set of ordinary differential equations that govern the fluid-solid flow.

Transonic Aerodynamics with Harmonic Balance

We now describe results obtained with the harmonic balance technique of Hall et al.,[77] as summarized in the Analysis section. Hall et al. consider the flowfield near the tip of a front-stage rotor for a high-pressure compressor.[77] The flow is modeled as two dimensional and the configuration is treated as an infinite blade row by imposing a suitable periodicity condition. The inlet Mach number and Reynolds number are specified to be 1.27 and the governing equations are the Navier-Stokes equations, closed with the Spalart-Allmaras turbulence model.[98] A baseline grid of H-O-H topology with 193×33 points is found to produce grid-converged

results. The complexity of the steady-state flowfield is captured in Fig. 12, where shock-shock and shock-boundary layer interactions are observed to occur.
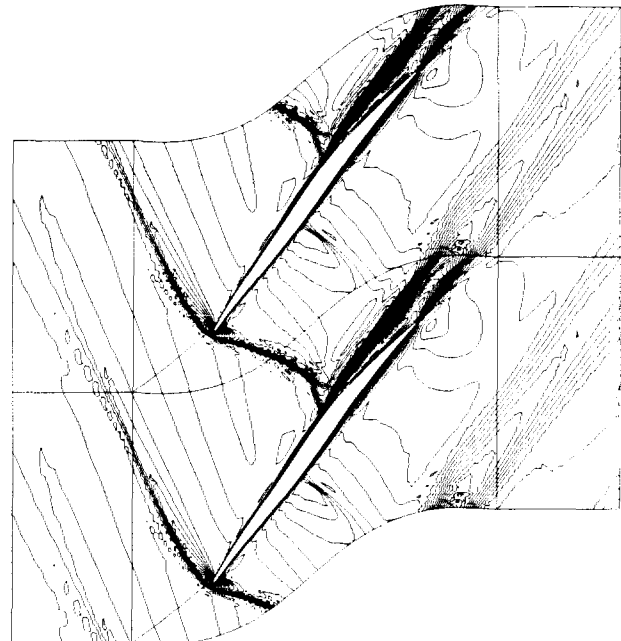

Fig. 12 Computed Mach number contours for transonic viscous flow through front stage compressor rotor (from Hall et al.[77] with permission). Two instances of spatially periodic flowfield shown for clarity.

Time-periodic unsteadiness is introduced by Hall et al. in the rotor flowfield by oscillating the rotors in pitch about their midchords with a reduced frequency of 1. While they report many results, we summarize their findings for the imaginary component of the first harmonic of the unsteady surface pressure, which has implications for aeroelastic stability.[77] Variations with respect to two parameters are examined: the pitch amplitude ($\bar{\alpha}$) and the interblade phase angle (σ). Pressure is nondimensionalized by inlet dynamic pressure (q_{inlet}), airfoil chord (c), and $\bar{\alpha}$ (to better

display nonlinear effects). For $\sigma = 30$ degrees, first harmonics of the unsteady pressure distributions are shown for different values of pitch amplitude and numbers of retained harmonics (N_{HB}) in Fig. 13. The first harmonic solution is rapidly convergent in N_{HB}, with 5 harmonics being sufficient to capture all details of the unsteady pressure distribution. Nonlinearity arises with increasing $\bar{\alpha}$, and are particularly noticeable when $\bar{\alpha}$ reaches 1 degree near a normalized airfoil surface position of 0.4. At this location, the unsteady pressure spike spreads out, a result of shock movement about this point.[77]
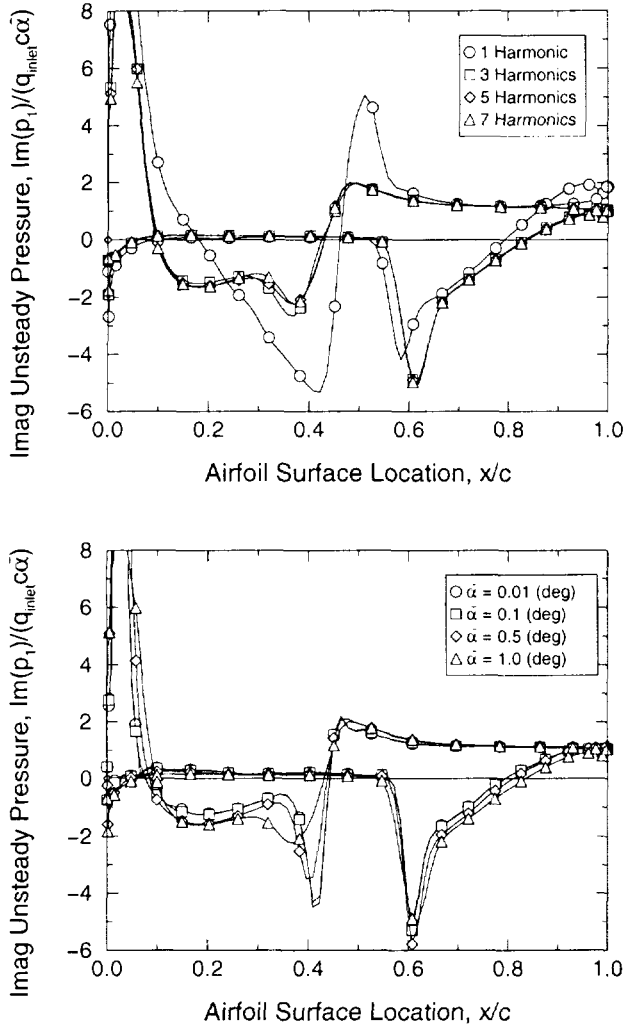

Fig. 13 First harmonic of unsteady pressure distribution for front stage compressor rotor airfoils vibrating in pitch. Top: Variation of number of retained harmonics for pitch amplitude of one degree. Bottom: Variation of pitch amplitude for $N_{HB} = 5$ (from Hall et al.[77] with permission).

Variation of the imaginary part of the first harmonic of the pitching moment yields a more dramatic indication of the role of nonlinearity. Blade stability is

achieved when this component of the integrated pitching moment is negative for all values of σ.[77] Results are displayed in Fig. 14, where it is seen that nonlinear aerodynamics serve to stabilize the flow when $\bar{\alpha}$ is increased to about 1 degree.
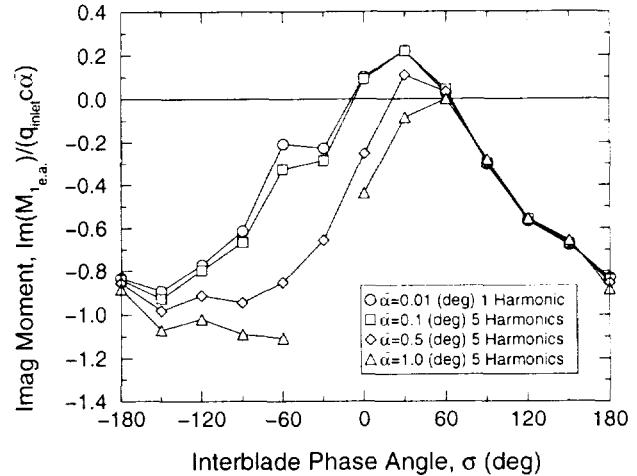

Fig. 14 Imaginary part of first harmonic of the blade pitching moment as a function of interblade phase angle (from Hall et al.[77] with permission).

The HB scheme is reported to be highly efficient, an order of magnitude faster than conventional time-accurate, time-integration schemes.[77] Converged results are found when 5 harmonics are retained, at a computational cost 7.5 times larger than that of steady-state analysis, per iteration. Convergence to a numerical solution is not obtained with the HB method when N_{HB} is increased to 7, a situation that is being further investigated at Duke University.

Thomas, Dowell and Hall are also applying the HB scheme to the study of limit-cycle oscillation in airfoils with structural coupling in the transonic regime.[78] This work is important in unraveling the role of moving shocks in the phenomenon of limit-cycle oscillation.

Concluding Remarks

The development of ROMs based on the time-domain version of the Volterra theory of nonlinear systems has been described, including continuous- and discrete-time versions of the theory. The basic objective of the theory is the identification of linearized and nonlinear kernel functions that capture the dominant response features of a nonlinear system. This is, in fact, a nonlinear Green's function method that provides a very natural and intuitive extension of well-understood linear phenomena into the nonlinear domain.

In the fields of unsteady aerodynamics and aeroelasticity, the use of influence coefficient functions, such as aerodynamic influence coefficient (AICs) functions and structural influence coefficient (SICs) functions

are routine. Since these influence coefficient functions are derived from Green's function concepts, the extension of these concepts into the nonlinear domain via the Volterra theory is quite natural and effective. In fact, these functions can be seen as a linear subset of a much broader nonlinear Volterra functional space.

While in its infancy for the analysis of large, spatially discrete systems, the Volterra method is currently under continued development. One of the encouraging applications presented is for a Navier-Stokes solution of a 2-D RAE airfoil in transonic flow using the CFL3D code with the Spalart-Allmaras turbulence model. First- and second-order kernels were computed for plunging motions of the airfoil. It was shown that the first-order kernel (that captures amplitude-dependent nonlinearities) was used successfully to predict the plunging response of the airfoil for large (nonlinear) plunging motions at a minute fraction of the cost of the full CFD solution. Another important result reviewed was an Euler solution of the AGARD 445.6 Aeroelastic Wing recently computed by Raveh et al.[14] using the EZNSS CFD code. It was shown that with pulse or step responses the full linearized frequency-domain generalized aerodynamic force matrices were reproduced at a fraction of the time and cost than that required by standard techniques.

The status of the Volterra-based ROM approach can be summarized as follows. The method has been used to show that discrete-time concepts, indeed digital signal processing concepts such as unit pulses and step inputs, are directly applicable to CFD codes. The method has also been shown to be a higher-level generalization of the standard linear methods in use today. This is beneficial, because it means that industry experts do not need to restructure their analysis process in order to introduce Volterra-based methods into their design algorithms. In addition, the nature of the method is such that it requires minimal, if any, modification to the CFD code of interest. Most unsteady aerodynamic or aeroelastic CFD codes already have various excitation inputs (e.g., sinusoidal) and extension to a Volterra-based ROM approach simply involves adding a pulse (or step) input to the suite of available inputs - the CFD code itself remains unchanged.

As for the challenges associated with the Volterra-based ROM approach, there is much work to be done. An important issue that needs to be addressed is the issue of modal superposition with respect to nonlinear effects. Although it is clear that a mode-by-mode excitation is a linearization of the aeroelastic process, it is important to understand the limitations of this approach. In addition, work continues on the development of a technique that provides simultaneous excitation to all modes, eliminating the linearization issue. Linearized state-space models are being developed using the CFD-based pulse responses. These state-space models can be incorporated directly into control system analysis, for example. These state-space matrices also sidestep the need to transform time-domain CFD loads into the frequency-domain only to transform the frequency-domain loads back into the time domain via rational function approximations. Using the Volterra approach, time-domain CFD-based information goes directly into creating time-domain state-space matrices, a more efficient process. But the ultimate challenge lies in the creation of nonlinear (bilinear) state-space matrices which are mathematically related to the Volterra kernels. Some work has been done in this area, but there is significantly more work that needs to be done.

The results reviewed in this paper demonstrate the viability of POD-based reduced order models for rapid analysis of aerodynamic and aeroelastic problems. The frequency-domain approach of Hall et al. has previously been shown[50] to predict accurately the linearized response of structurally coupled airfoils in transonic flow. As is typical in the use of POD-based ROMs, the computational cost of constructing low-order models through the frequency-domain approach is dominated by sampling (snapshot collection). Solutions are required for discrete distributions of frequency in each of the characterisitc modes of deformation (pitch and plunge in the case of the structurally supported airfoil). The cost of obtaining a large number of snapshots can exceed that required to execute a small number of general simulations. However, several important benefits in the application of POD to aeroelastic problems are suggested by the work of Hall et al. for 2-D airfoils[50] and Thomas et al. for 3-D wings.[73] Following the one-time construction of a very low-order aeroelastic model, effects of parametric variations in the structural dynamics model can be rapidly assessed. Furthermore, the consequences of more fundamental changes to the structural model, such as freeplay,[55] can be understood with greater clarity. The extension to higher level multi-disciplinary applications, e.g., aeroservoelasticity or design with aeroelastic constraints, may be made practical by the presence of low-order models. Lastly, the frequency domain POD represents an efficient and accurate compression of the salient dynamic characteristics of the aeroelastic system. In summary, the efficiencies of POD-based ROMs are realized when system properties can be characterized and observed once for ROM construction and then be allowed to vary in new ways compatible with the previous observations.

Application of the subspace projection method to the steady-state analysis of inviscid, compressible flow over a bump has yielded significant insight into the suitability of POD-based methods for nonlinear aerodynamic and aeroelastic analyses. By collecting a nominal number of solution samples over a two-parameter space, defined by bump amplitude and

freestream Mach number, a POD-based ROM was constructed that preserved the nonlinear transition of supersonic flow states towards transonic states. Not surprisingly, we observed that the range of validity (as measured by a residual norm of the full system) of the ROM decreased as the number of retained modes was decreased. Interestingly, validity was longest lasting in the linear region of the parameter space (small amplitude for given Mach number), suggesting that low-energy modes were important in the accurate capture of nonlinear behavior, as also seen in the dynamic analysis. Computation of ROM solutions required approximately two orders of magnitude fewer function evaluations, which allowed a much more rapid and detailed exploration of the previously sampled solution space. We speculate that such ROMs are more reliable and useful than interpolation, although this should be documented. Aside from the potential advantages of data compression (i.e., keeping fewer modes than fully represented by the snapshot data), which could be significant in large systems characterized by large numbers of parameters, the ROM/POD provides a compact set of degrees of freedom that can be varied to evaluate sensitivities, optimal configurations, and system stability, in a manner based on the discrete equations of the full system.

Unsteady aerodynamic solutions were also obtained with the subspace projection method at a significant computational savings over standard analysis. Results were reported for the response of a supersonic flow over a bump, like that described in the steady analysis, whose amplitude varied sinusoidally in time. Following construction of a reduced-order model, the time-dependent character of the reduced-order system was accurately and efficiently computed with a sub-iterate form of the implicit Crank-Nicolson scheme. Time-dependent solutions of the ROM were computed an order of magnitude faster than full-system analysis. As true of the steady-state analysis, the computational cost associated with application of the POD-based ROM was dominated by the cost of data sampling used in ROM construction. The relative significance of the sampling cost can be minimized by constructing hybrid ROMs that account for frequency and amplitude variations, and which are robust over a wider range of possible bump dynamics.

Efficiency of the subspace projection technique was derived from two sources: decrease of the number of variables that characterize the system, and increase of allowable time step. In the bump problem, the number of variables was decreased by three orders of magnitude (40,000 to about 10). The method was not three orders of magnitude faster, however, since evaluations of the full-system source term ($\mathbf{R}$ in (9)) were required with this approach. For steady analysis, full-system evaluations were employed in the construction of the ROM Jacobian, and in unsteady analysis, full-system

evaluations were also necessary in the computation of dynamic residuals. With the POD-based ROM, computational work associated with implicit portions (i.e., left-hand sides) of system equations is virtually eliminated. Thus, the subspace projection method is particularly well suited for implicit formulations of nonlinear problems, such as steady-state, sensitivity and bifurcation analyses. For unsteady problems, it was also found that time steps allowed by POD-based ROMs were an order of magnitude larger than that allowed by explicit, full-system analysis. The current approach should be compared to the computation of a relevant viscous flow using a standard implicit technique to determine potential savings for a practical problem.

Once sampling identifies the most energetic POD modes, other techniques are available with which the governing equations can be reduced in order; for example, Galerkin projection can be used to fully project the governing equations. The relative merits and demerits of the Galerkin and subspace projection methods are described in the Analysis section. Currently, the Galerkin approach is being used by Cizmas and Palacios to develop a small set of ordinary differential equations representative of jet flow in a solid/liquid mixture. A subspace projection method is also being adapted by Lucia, King, Beran and Oxley[97] to treat a CFD problem for which the computational domain is decomposed to isolate a moving shock. Other techniques, such as collocation, should be explored that may allow the POD modes to be used in a more efficient manner than subspace projection, but with perhaps greater flexibility than Galerkin projection.

An alternative approach to POD based on harmonic balance has been proposed by Hall, Thomas and Clark[77] for the efficient computation of complex, time-periodic systems. With their technique, the response of a rotor flowfield to rotor pitch oscillation was accurately simulated, and behaviors related to shock movement and shock/boundary-layer interaction were captured. By using a low-order representation of system dynamics, the harmonic balance technique yielded response predictions approximately an order of magnitude faster than with traditional techniques.

In closure, several methods have been described in this paper that offer new potential for the computational analysis of large, nonlinear systems. These methods share a common reliance on existing numerical techniques, and in this sense do not replace traditional methods. Instead, reduced-order and harmonic-balance techniques provide existing methods with a higher level of algorithmic operation that enables more sophisticated computations. For example, a POD-based ROM of a discretized convection-diffusion-reaction (CDR) system was described and shown capable of determining a variety of important characteristics of the nonlinear system, including nonlinear static behavior, bifurcation to limit-cycle behavior,

and sensitivity to changes in system parameters. The CDR problem serves as an analog for the study of the aeroelastic properties of a wing, including static analysis (e.g., determination of a control-surface reversal speed), dynamic analysis (e.g., prediction of a limit-cycle oscillation amplitude), bifurcation analysis (e.g., at what reduced velocities of the nonlinear system does flutter occur), and sensitivity analysis (e.g., how do aeroelastic behaviors depend on structural parameters). Aeroelastic analysis of all these bahaviors in a manner that is useful for structural or aeroservoelastic design is well beyond traditional methods. It is by answering more difficult questions, typically in the framework of multidisciplinary analysis, that ROM techniques become attractive, if not necessary.

There are several challenges that need to be overcome before ROM methods can be routinely applied to practical problems. We group these difficulties into three categories: construction, generality, and accuracy assessment. Which ROM method should be applied to a particular problem will probably depend on the relative significance of these issues to the specified problem. In the first category, work needs to be carried out to understand what response behaviors should be included in the construction of ROMs to model robustly the response characteristics of systems with large numbers of parameters. In other words, how much sampling is required for a particular system? Generality of the ROM approach is also an important issue. Is the approach readily or stubbornly extendable to different problems involving different simulation tools? Can the ROM approach function with modern, shock-capturing, CFD methods that incorporate turbulence models and deforming meshes with unstructured or structured/overset connectivities? And finally, the accuracy of ROMs must be quantifiable for confident use. Systematic procedures must be developed (such as residual monitoring) to self-check ROM solutions and highlight conditions upon which ROMs should be re-constructed.

Acknowledgements

References

[1]Silva, W. A., *Discrete-Time Linear and Nonlinear Aerodynamic Impulse Responses for Efficient CFD Analyses*, Ph.D. thesis, College of William & Mary, December 1997.

[2]Bisplinghoff, R. L. and Ashley, H., *Principles of Aeroelasticity*, Dover Publications, Inc., New York, 1975.

[3]Giesing, J. P., Kalman, T. P., and Rodden, W. P., "Subsonic Unsteady Aerodynamics for General Configurations, Part I. Direct Application of the Nonplanar Doublet Lattice Method," Report AFFDL-TR-71-5, Vol. I, November 1971.

[4]Leishman, J. and Crouse, G., "A State-Space Model of Unsteady Aerodynamics in a Compressible Flow for Flutter Analyses," AIAA Paper 89-0022, January 1989.

[5]Nixon, D., *Alternative Methods for Modeling Unsteady Transonic Flows, Unsteady Transonic Aerodynamics*, Vol. 120 of Progress in Astronautics and Aeronautics, AIAA, 1989.

[6]Reisenthel, P. H., "Development of a Nonlinear Indicial Model for Maneuvering Fighter Aircraft," AIAA Paper 96-0896, January 1996.

[7]Marques, F. and Anderson, J., "Modelling and Identification of Non-Linear Unsteady Aerodynamic Loads by Neural Networks and Genetic Algorithms," ICAS Paper 96-7.1.1, September 1996, pp. 243–251.

[8]Govind, G. and Ramamoorthy, P. A., "Multi-layered Neural Networks and Volterra Series: The Missing Link," IEEE International Conference on Systems Engineering, August 9-11, 1990, pp. 633–636.

[9]Soloway, D. I. and Bialasiewicz, J. T., "Neural Network Modeling of Nonlinear Systems Based on Volterra Series Extension of a Linear Model," IEEE International Symposium on Intelligent Control, Glasgow, Scotland.

[10]Dowell, E. H., Hall, K. C., and Romanowski, M. C., "Eigenmode Analysis in Unsteady Aerodynamics: Reduced Order Models," *Applied Mechanical Review*, Vol. 50, No. 6, June 1997, pp. 371–385.

[11]Baker, M. L., *Model Reduction of Large, Sparse, Discrete Time Systems with Application to Unsteady Aerodynamics*, Ph.D. thesis, University of California at Los Angeles, 1996.

[12]Seidel, D. A., Bennett, R. M., and Ricketts, R. H., "Some Recent Applications of XTRAN3S," AIAA Paper 83-1811.

[13]Lee-Rausch, E. M. and Batina, J. T., "Wing Flutter Computations Using an Aerodynamic Model Based on the Navier-Stokes Equations," *Journal of Aircraft*, Vol. 33, No. 6, pp. 1139–1148.

[14]Raveh, D., Levy, Y., and Karpel, M., "Aircraft Aeroelastic Analysis and Design Using CFD-Based Unsteady Loads," AIAA Paper 2000-1325, April 2000.

[15]Silva, W. A. and Raveh, D. E., "Development of Aerodynamic/Aeroelastic State-Space Models from CFD-Based Pulse Responses," AIAA Paper No. 2001-1213 (to be presented at the 42nd Structures, Structural Dynamics, and Materials Conference, Seattle, WA.

[16]Diaz, H., *Modeling of Nonlinear Systems from Input-Output Data*, Ph.D. thesis, Rensselaer Polytechnic Institute, 1986.

[17]Pitas, I. and Venetsanopoulos, A. N., *Nonlinear Digital Filters: Principles and Applications*, Kluwer Academic Publishers, 1990.

[18]Ueda, T. and Dowell, E. H., "Flutter Analysis Using Nonlinear Aerodynamic Forces," *Proceedings of the 23rd AIAA/ASME/ASCE/AHS Structures, Structural, Dynamics, and Materials Conference, New Orleans, LA, AIAA Paper 82-0728-CP*, pp. 462–481.

[19]Tobak, M. and Pearson, W. E., "A Study of Nonlinear Longitudinal Dynamic Stability," NASA Technical Dissertation R-209.

[20]Jenkins, J. E., "Relationships Among Nonlinear Aerodynamic Indicial Response Models, Oscillatory Motion Data, and Stability Derivatives," Proceedings of the AIAA Atmospheric Flight Mechanics Conference, Boston, MA, AIAA Paper 89-3351-CP.

[21]Stalford, H., Baumann, W. T., Garrett, F. E., and Herdman, T. L., "Accurate Modeling of Nonlinear Systems Using Volterra Series Submodels," American Control Conference, Minneapolis, MN, June 1987.

[22]Rugh, W. J., *Nonlinear System Theory, The Volterra-Wiener Approach*, The John Hopkins University Press, 1981.

[23]Clancy, S. J. and Rugh, W. J., "A Note on the Identification of Discrete-Time Polynomial Systems," *IEEE Transactions on Automatic Control*, Vol. AC-24, No. 6.

[24]Schetzen, M., "Measurement of the Kernels of a Nonlinear System of Finite Order," *International Journal of Control*, Vol. 1, No. 3, pp. 251–263.

[25]Boyd, S. P., Chang, Y. S., and Chua, L. O., "Measuring Volterra Kernels," *IEEE Transactions on Circuits and Systems*, Vol. CAS-30, No. 8, August 1983.

[26]Reisenthel, P. H., "Prediction of Unsteady Aerodynamic Forces via Nonlinear Kernel Identification," presented at the International Forum on Aeroelasticity and Structural Dynamics, Williamsburg, VA.

[27]Tromp, J. C. and Jenkins, J. E., "A Volterra Kernel Identification Scheme Applied to Aerodynamic Reactions," AIAA Paper 90-2803.

[28]Rodriguez, E. A., *Linear and Nonlinear Discrete-Time State-Space Modeling of Dynamic Systems for Control Applications*, Ph.D. thesis, Purdue University, December 1993.

[29]Silva, W. A., "Application of Nonlinear Systems Theory to Transonic Unsteady Aerodynamic Responses," *Journal of Aircraft*, Vol. 30, No. 5, September-October 1993, pp. 660–668.

[30]Silva, W. A., "Extension of a Nonlinear Systems Theory to Transonic Unsteady Aerodynamic Responses," AIAA Paper 93-1590, April 1993.

[31]Karhunen, K., *Zur Spektral Theorie Stochastischer Prozesse*, Ann. Acad. Sci. Fennicae, Ser, 1946.

[32]Loève, M., *Functions Aleatoire de Second Ordre*, C. R. Academie des Sciences, Paris, France, 1945.

[33]Ahmed, N. and Goldstein, M. H., *Orthogonal Transforms for Digital Signal Processing*, Springer-Verlag, 1975.

[34]Lumley, J. L., "The Structure of Inhomogeneous Turbulence," *Proceedings of the International Colloquium on the Fine Scale Structure of the Atmosphere and its Influence on Radio Wave Propagation*, edited by A. M. Yaglom, Dokl. Akad. Nauk SSSR, Moscow, 1967, pp. 166–178.

[35]Bakewell, P. and Lumley, J. L., "Viscous Sublayer and Adjacent Wall Region in Turbulent Pipe Flows," *Physics of Fluids*, Vol. 10, 1967, pp. 1880–1889.

[36]Berkooz, G., Holmes, P., and Lumley, J. L., "The Proper Orthogonal Decomposition in the Analysis of Turbulent Flows," *Annual Reviews of Fluid Mechanics*, Vol. 25, 1993, pp. 539–575.

[37]Masri, S. F., Smyth, A. W., and Traina, M.-I., "Probabilistic Representation and Transmission of Nonstationary Processes in Multi-Degree-of-Freedom Systems," *Transactions of the ASME*, Vol. 65, June 1998, pp. 398–409.

[38]Jeong, S.-W., Bienkiewicz, B., and Ham, H.-J., "Proper Orthogonal Decomposition of Building Wind Pressure Specified at Non-Uniformly Distributed Pressure Taps," *Journal of Wind Engineering and Industrial Aerodynamics*, Vol. 87, 2000, pp. 1–14.

[39]Krysl, P., Lall, S., and Marsden, J. E., "Dimensional Model Reduction in Non-Linear Finite Element Dynamics of Solids and Structures," *submitted to the International Journal for Numerical Methods in Engineering*, 2000.

[40]S. A. Mortara, J. C. S. and Beran, P. S., "A Proper Orthogonal Decomposition Technique for the Computation of Nonlinear Panel Response," AIAA Paper 2000-1936, 2000.

[41]Moin, P. and Moser, R. D., "Characteristic-Eddy Decomposition of Turbulence in a Channel," *Journal of Fluid Mechanics*, Vol. 200, 1989, pp. 471–509.

[42]Sirovich, L., "Turbulence and the Dynamics of Coherent Structures. Part I: Coherent Structures," *Quarterly of Applied Mathematics*, Vol. 45, No. 3, October 1987, pp. 561–571.

[43]Deane, A. E., Kevrekidis, I. G., Karniadakis, G. E., and Orszag, S. A., "Low-Dimensional Models for Complex Geometry Flows: Application to Grooved Channels and Circular Cylinders," *Physics of Fluids*, Vol. 3, No. 2, October 1991, pp. 2337–2354.

[44]Park, H. M. and Cho, D. H., "The Use of the Karhunen-Loeve Decomposition for the Modeling of Distributed Parameter Systems," *Chemical Engineering Science*, Vol. 51, No. 1, 1996, pp. 81–89.

[45]Park, H. M. and Lee, M. W., "An Efficient Method of Solving the Navier-Stokes Equation for Flow Control," *International Journal for Numerical Methods in Engineering*, Vol. 41, 1998, pp. 1133–1151.

[46]Rediniotis, O. K., Ko, J., Yue, X., and Kurdila, A. J., "Synthetic Jets, their Reduced Order Modeling and Applications to Flow Control," *37th Aerospace Sciences Meeting and Exhibit, Reno, N.V.*, AIAA Paper 99-1000, January 1999.

[47]Tang, K. Y., Graham, W. R., and Peraire, J., "Active Flow Control Using a Reduced Order Model and Optimum Control," AIAA Paper 96-1946, 1996.

[48]Romanowski, M. C., "Reduced Order Unsteady Aerodynamic and Aeroelastic Models Using Karhunen-Loeve Eigenmodes," *6th AIAA/USAF/NASA/ISSMO Symposium on Multidisciplinary Analysis and Optimization, Bellevue WA*, AIAA 96-3981-CP, September 1996, pp. 7–13.

[49]Kim, T., "Frequency-Domain Karhunen-Loeve Method and Its Application to Linear Dynamic Systems," *AIAA Journal*, Vol. 36, No. 11, November 1998, pp. 2117–2123.

[50]Hall, K. C., Thomas, J. P., and Dowell, E. H., "Proper Orthogonal Decomposition Technique for Transonic Unsteady Aerodynamic Flows," *AIAA Journal* (also AIAA Paper 99-0655), Vol. 38, No. 10, October 2000, pp. 1853–1862.

[51]Beran, P. S., Huttsell, L. J., Buxton, B. J., Noll, C., and Osswald, G., "Computational Aeroelasticity Techniques for Viscous Flow," *CEAS/AIAA/ICASE/NASA Langley International Forum on Aeroelasticity and Structural Dynamics, Williamsburg, VA*, June 1999.

[52]Pettit, C. L. and Beran, P. S., "Reduced-Order Modeling for Flutter Prediction," *41st AIAA/ASCE/AHS/ASC Structures, Structural Dynamics and Materials Conference, Atlanta, GA*, AIAA Paper 2000-1446-CP, April 2000.

[53]Pettit, C. L. and Beran, P. S., "Application of Proper Orthogonal Decomposition to the Discrete Euler Equations," *submitted to the International Journal for Numerical Methods in Engineering*, December, 2000.

[54]Beran, P. S. and Pettit, C. L., "Prediction of Nonlinear Panel Response Using Proper Orthogonal Decomposition," *to be presented at the 42nd AIAA/ASCE/AHS/ASC Structures, Structural Dynamics and Materials Conference, Bellvue, WA*, April 2001.

[55]Dowell, E. H., Thomas, J. P., and Hall, K. C., "Transonic Limit Cycle Oscillation Analysis Using Reduced Order Modal Aerodynamic Models," *to be presented at the 42nd AIAA/ASCE/AHS/ASC Structures, Structural Dynamics and Materials Conference, Bellvue, WA*, April 2001.

[56]Volterra, V., *Theory of Functionals and of Integral and*

Integro-Differential Equations, Dover Publications, Inc., New York, 1959.

[57]Schetzen, M., *The Volterra and Wiener Theories of Nonlinear Systems*, John Wiley & Sons, 1980.

[58]Bendat, J. S., *Nonlinear System Analysis & Identification from Random Data*, Wiley-Interscience, 1990.

[59]Silva, W. A., "Reduced-Order Models Based on Linear and Nonlinear Aerodynamic Impulse Responses," *CEAS/AIAA/ICASE/NASA Langley International Forum on Aeroelasticity and Structural Dynamics, Williamsburg, VA*, June 1999, pp. 369–379.

[60]Boyd, S. P., *Volterra Series: Engineering Fundamentals*, Ph.D. thesis, University of California, Berkeley, 1985.

[61]Oppenheim, A. V. and Schafer, R. W., *Discrete-Time Signal Processing (Prentice Hall Signal Processing Series)*, Prentice Hall, Englewood Cliffs, NJ.

[62]Marzocca, P., Librescu, L., and Silva, W. A., "Nonlinear Stability and Response of Lifting Surfaces via Volterra Series," *presented at the 20th International Congress of Theoretical and Applied Mechanics, Chicago, IL*, 27 August - 2 September 2000.

[63]Prazenica, R., Kurdila, A., and Silva, W. A., "Multiresolution Methods for Representation of Volterra Series and Dynamical Systems," AIAA Paper 2000-1754, April 2000.

[64]Holmes, P., Lumley, J. L., and Berkooz, G., *Turbulence, Coherent Structures, Dynamical Systems and Symmetry*, Cambridge University Press, 1996.

[65]Newman, A. J., "Model Reduction Via the Karhunen-Loeve Expansion Part 1: An Exposition," Tech. Rep. T.R. 96-32, Institute for Systems Research, University of Maryland, 1996.

[66]Childers, D. G., *Probability and Random Processes*, McGraw-Hill, 1997.

[67]Mallat, S. A., *A Wavelet Tour of Signal Processing*, Academic Press, San Diego, 1998.

[68]Strang, G., *Linear Algebra and Its Applications*, 3rd ed., 1988.

[69]Romanowski, M. C. and Dowell, E. H., "Aeroelastic Analysis of an Airfoil Using Eigenmode Based Reduced Order Unsteady Aerodynamics," *36th AIAA/ASME/ASCE/AHS/ASC Structures, Structural Dynamics, and Materials Conference, New Orleans, LA*, AIAA Paper 95-1380-CP, April 1995, pp. 1863–1870.

[70]Beran, P. S. and Morton, S. A., "Continuation Method for Calculation of Transonic Airfoil Flutter Boudnaries," *Journal of Guidance, Control and Dynamics*, Vol. 20, No. 6, December 1997, pp. 1165–1171.

[71]Morton, S. A. and Beran, P. S., "Hopf-Bifurcation Analysis of Airfoil Flutter at Transonic Speeds," *Journal of Aircraft*, Vol. 36, No. 2, 1999, pp. 421–429.

[72]Beran, P. S., "A Domain-Decomposition Method for Airfoil Flutter Analysis," AIAA Paper 99-0098, January 1998.

[73]Thomas, J. P., Dowell, E. H., and Hall, K. C., "Three-Dimensional Transonic Aeroelasticity Using Proper Orthogonal Decomposition Based Reduced Order Models," *to be presented at the 42nd AIAA/ASCE/AHS/ASC Structures, Structural Dynamics and Materials Conference, Bellvue, WA*, April 2001.

[74]Slater, J. C., Pettit, C. L., and Beran, P. S., "In-Situ Subspace Evaluation in Reduced Order Modelling," *to be presented at the 42nd AIAA/ASCE/AHS/ASC Structures, Structural Dynamics and Materials Conference, Bellvue, WA*, April 2001.

[75]Beran, P. S. and Pettit, C. L., "Computational Aeroelasticity for MDO," *Advances in Computational Engineering and Sciences 2000 (Collection of Papers presented at the ICES '2K Conference)*, edited by S. N. Atluri and F. W. Brust, Vol. 2, Tech Science Press, August 2000, pp. 1562–1567.

[76]Isaacson, E. and Keller, H. B., *Analysis of Numerical Methods*, John Wiley & Sons, Inc, New York, 1966.

[77]Hall, K. C., Thomas, J. P., and Clark, W. S., "Computation of Unsteady Nonlinear Flows in Cascades Using a Harmonic Balance Technique," *9th International Symposium on Unsteady Aerodynamics, Aeroacoustics and Aeroelasticity of Turbomachines and Propellers, Lyon, France*, September 4-8, 2000.

[78]Thomas, J. P., Dowell, E. H., and Hall, K. C., "Nonlinear Inviscid Aerodynamic Effects on Transonic Divergence, Flutter and Limit Cycle Oscillations," *to be presented at the 42nd AIAA/ASCE/AHS/ASC Structures, Structural Dynamics and Materials Conference, Bellvue, WA*, April 2001.

[79]Guruswamy, G. P. and Tu, E. L., "Navier-Stokes Computations on Flexible Advanced Transport Wings in Transonic Regime," *Journal of Aircraft*, Vol. 33, No. 3, 1996, pp. 576–581.

[80]Gordnier, R. E. and Melville, R. B., "Accuracy Issues for Transonic Wing Flutter Using 3-D Navier-Stokes," *Proceedings of the 39th AIAA/ASME/ASCE/AHS/ASC Structures, Structural Dynamics, and Materials Conference, Long Beach, CA*, AIAA Paper 98-1729-CP, April 1998.

[81]Parker, T. S. and Chua, L. O., *Practical Numerical Algorithms for Chaotic Systems*, Springer-Verlag, Inc., New York, NY, 1989.

[82]Nayfeh, A. and Balachandran, B., *Applied Nonlinear Dynamics*, John-Wiley and Sons, Inc., New York, NY, 1995.

[83]Seydel, R., *From Equilibrium to Chaos: Practical Bifurcation and Stability Analysis*, Elsevier Science, Inc., 1988.

[84]Holodniok, M. and Kubicek, M., "DERPER - An Algorithm for the Continuation of Periodic Solutions in Ordinary Differential Equations," *Journal of Computational Physics*, Vol. 55, 1984, pp. 254–267.

[85]Beran, P. S., "Computation of Limit-Cycle Oscillation Using a Direct Method," AIAA Paper 99-1462, April 1999.

[86]Rumsey, C. L., Biedron, R. T., and Thomas, J. L., "CFL3D: Its History and Some Recent Applications," NASA TM 112861, May, 1997.

[87]Raveh, D. E., Levy, Y., and Karpel, M., "Structural Optimization Using Computational Aerodynamics," International Forum on Aeroelasticity and Structural Dynamics, Williamsburg, VA, pp. 469–481.

[88]Isogai, K., "On the Transonic-Dip Mechanism of Flutter of Sweptback Wing," *AIAA Journal*, Vol. 17, No. 7, 1979, pp. 793–795.

[89]Ehlers, F. E. and Weatherhill, W. H., "A Harmonic Analysis Method for Unsteady Transonic Flow and Its Application to the Flutter of Airfoils," NASA CR-3537, May 1982.

[90]Edwards, J. W., Bennett, R. M., Whitlow Jr., W., and Seidel, D. A., "Time-Marching Transonic Flutter Solutions Including Angle-of-Attack Effects," *Journal of Aircraft*, Vol. 20, No. 11, 1983, pp. 899–906.

[91]Lee-Rausch, E. M. and Batina, J. T., "Wing Flutter Boundary Prediction Using Unsteady Euler Aerodynamic Method," *Journal of Aircraft*, Vol. 32, No. 2, 1995, pp. 416–422.

[92]Harten, A., "High Resolution Schemes for Hyperbolic Conservation Laws," *J. Comp. Phys.*, Vol. 49, 1983, pp. 357–393.

[93]Yee, H. C., "A Class of High-Resolution Explicit and Implicit Shock Capturing Methods," NASA TM-101088, 1989.

[94]Strang, W. Z., Tomaro, R. F., and Grismer, M. J., "The Defining Methods of Cobalt60: A Parallel, Implicit, Unstructured Euler/Navier-Stokes Flow Solver," AIAA Paper 99-0786.

[95]Heinemann, R. F. and Poore, A. B., "Multiplicity, Stability and Oscillatory Dynamics of the Tubular Reactor," *Chem. Eng. Sci.*, 1981.

[96]Roose, D. and Hlavacek, V., "Numerical Computation of Hopf Bifurcation Points for Parabolic Diffusion-Reaction Differential Equations," *Applied Mathematics*, Vol. 43, No. 5, October 1983, pp. 1075–1085.

[97]Lucia, D., King, P., Beran, P., and Oxley, M., "Reduced Order Modeling for a Quasi 1-D Nozzle with Moving Shocks," *submitted for presentation at the 15th AIAA Computational Fluid Dynamics Conference, Anaheim, CA*, June 2001.

[98]Spalart, P. R. and Allmaras, S. R., "A One Equation Turbulence Model for Aerodynamic Flows," AIAA Paper 92-0439, 1992.

AMERICAN INSTITUTE OF AERONAUTICS AND ASTRONAUTICS PAPER 2001-0853